CD206^{+}IL-4Rα^{+} MACROPHAGES ARE DRIVERS OF ADVERSE CARDIAC REMODELING IN ISCHEMIC CARDIOMYOPATHY

Qiongxin Wang, PhD;[1,2,3] Mohamed Ameen Ismahil, PhD;[1,3] Yujie Zhu, MD, PhD;[1,3] Gregg Rokosh, PhD;[1,3] Tariq Hamid, PhD;[1,3] Guihua Zhou, MD, PhD;[1] Steven M. Pogwizd, MD;[1] Sumanth D. Prabhu, MD[1,3]

[1]Division of Cardiovascular Disease, University of Alabama at Birmingham, Birmingham, AL
[2]Department of Cardiology, Zhongnan Hospital of Wuhan University, Wuhan, China,
[3]Division of Cardiology, Department of Medicine, Washington University School of Medicine, St. Louis, MO

Running title: Alternatively activated macrophages promote adverse cardiac remodeling

Corresponding Author:

Sumanth D. Prabhu, MD
Lewin Distinguished Professor and Chief
Division of Cardiology
Washington University School of Medicine
660 S. Euclid Ave
CB 8086
St. Louis, MO 63110
Tel: 314-362-8908
Fax: 314-454-5550
Email: prabhu@wustl.edu

NONSTANDARD ABBREVIATIONS AND ACRONYMS

LV	left ventricular
MI	myocardial infarction
HF	heart failure
EF	ejection fraction
EDV	end-diastolic volume
ESV	end-systolic volume
LVAD	left ventricular assist device
BMDM	bone marrow-derived macrophage
cMSC	cardiac mesenchymal stem cell
ASO	antisense oligonucleotide
CCR2	C-C motif chemokine receptor 2
IL	interleukin
TGF-β	tumor growth factor-β
Arg1	arginase 1
FIZZ	found in inflammatory zone
Col	collagen
PDGF	platelet-derived growth factor
α-SMA	α-smooth muscle actin
NICD	Notch intracellular domain

ABSTRACT

BACKGROUND: Cardiac CD206^{+} macrophages expand acutely after myocardial infarction (MI) to promote wound healing; however, their role in chronic heart failure (HF) is unknown. We tested the hypothesis that cardiac CD206^{+} macrophages expressing interleukin(IL)-4Rα are key drivers of adverse left ventricular (LV) remodeling in HF.

METHODS AND RESULTS: Adult male C57BL/6 mice underwent non-reperfused MI to induce HF, or sham operation, and cardiac macrophages were profiled using flow cytometry. As compared to sham, CD206^{+} macrophages steadily expanded in post-MI hearts during LV remodeling, such that at 8 w post-MI they comprised ~85% of all macrophages. These macrophages were robustly proliferative and predominantly C-C motif chemokine receptor (CCR2)$^{-}$ and major histocompatibility complex (MHC)II^{hi}, with >90% of CD206^{+}CCR2^{-} macrophages expressing the resident macrophage marker LYVE-1. CD206^{+} macrophage abundance correlated with LV dysfunction and fibrosis. Nearly half of CD206^{+} macrophages expressed IL-4Rα, and the majority of CD206^{+}IL-4Rα^{+} macrophages co-expressed the pro-fibrotic protein found in inflammatory zone (FIZZ)1. IL-4-polarized bone marrow derived CD206^{+} macrophages also exhibited marked upregulation of FIZZ1 and induced FIZZ1-dependent myofibroblast differentiation of cardiac mesenchymal stem cells (cMSCs), in part related to DLL-4/Jagged1-Notch1 signaling. Intramyocardial adoptive transfer of M[IL-4], but not M[IL-10], CD206^{+} macrophages to naïve mice, induced progressive LV remodeling over 4 weeks, increasing fibrosis, cardiomyocyte hypertrophy, and apoptosis. Myeloid-specific IL-4Rα gene deletion in established HF (initiated 4 w post-MI) in IL-4R$\alpha^{f/f}$LysM-Cre^{ERT2} mice significantly reduced CD206^{+} macrophage proliferation and effectively depleted CD206^{+}IL-4Rα^{+} cardiac macrophages. This was associated with abrogation of LV remodeling progression, reduction of cardiac fibrosis, and improved neovascularization. *In vivo* IL-4Rα gene silencing in mice with established HF effectively depleted cardiac CD206^{+}IL-4Rα^{+} macrophages and reversed LV

remodeling, improving fibrosis, neovascularization, and dysfunction, and suppressed both local and systemic inflammation. Lastly, alternatively activated $CD206^+$ and $CD163^+$ macrophages were significantly expanded in human failing hearts and correlated with fibrosis. The majority of $CD163^+$ macrophages expressed IL-4Rα and FIZZ3, the human homolog of FIZZ1.

CONCLUSION: Cardiac $CD206^+$IL-4Rα^+ macrophages proliferate and expand in HF and are key mediators of pathological remodeling and fibrosis, in part through the secretion of FIZZ1. Inhibition of $CD206^+$ macrophage IL-4Rα signaling alleviates LV remodeling in ischemic cardiomyopathy.

Key Words: $CD206^+$ macrophages; fibrosis; heart failure; interleukin 4 receptor-α; inflammation

CLINICAL PERSPECTIVE

What is new?

- In the failing heart after myocardial infarction (MI), CD206^{+} macrophages, primarily CCR2^{-}, MHCII^{hi}, and LYVE1^{+}, robustly proliferate with a subpopulation expressing IL-4Rα; myeloid-specific IL-4Rα deletion or IL-4Rα silencing *in vivo* tempered CD206^{+} macrophage proliferation and alleviated LV dysfunction, fibrosis, and remodeling.
- M[IL-4] CD206^{+} bone-marrow derived macrophages induced upregulation of *Fizz1,* and FIZZ1-dependent cardiac mesenchymal myofibroblast differentiation; intramyocardial adoptive transfer of M[IL-4] macrophages induced cardiac remodeling and fibrosis.
- Humans exhibit expansion of alternatively activated macrophages in the failing heart marked by CD206 and CD163 expression, with predominance of a subpopulation expressing IL-4Rα and Fizz3, the human homolog of *Fizz1*.

What are the clinical implications?

- An expanded pool of alternatively activated CD206^{+}IL-4Rα^{+} cardiac macrophages are key drivers of LV remodeling in heart failure, inducing an immuno-fibrotic and para-inflammatory response in part dependent on FIZZ1.
- Targeting IL-4 signaling in CD206^{+} macrophages represents a potential therapeutic approach to limit long-term cardiac remodeling in heart failure.

INTRODUCTION

Heart failure (HF) is characterized by local and systemic inflammation.[1] In ischemic cardiomyopathy, activated macrophages expand in the failing myocardium and contribute to tissue injury and adverse left ventricular (LV) remodeling.[1-5] Cardiac macrophages may be classified as C-C motif chemokine receptor (CCR2)$^{-}$ resident macrophages that are embryonically derived and maintained independent of blood monocytes, and CCR2^{+} macrophages that are derived from monocyte recruitment.[6-8] Acutely after myocardial infarction (MI), resident CCR2^{-} macrophages are lost and replaced by Ly6C^{hi}CCR2^{+} monocytes and inflammatory CCR2^{+} macrophages that later transition to reparative macrophages to facilitate wound healing, accompanied by attendant proliferation of surviving resident macrophage populations.[3,6,9-11] Notably, in chronic ischemic cardiomyopathy, well after MI healing, the expanded cardiac macrophage pool stems from both locally proliferating resident macrophages and recruited CCR2^{+} monocytes,[2,3,5,6,12] with overall predominance of locally sourced (CCR2^{-}) cells.[3,5,12] CCR2^{+} macrophage abundance correlates with adverse LV remodeling in human HF,[2] whereas inhibiting CCR2^{+} monocyte infiltration sub-acutely after MI improves LV remodeling in mice,[5] identifying CCR2 as a potential therapeutic target. In contrast, the roles of locally sourced macrophage populations in the pathogenesis of LV remodeling in established HF are poorly defined.

Resident cardiac macrophages express several marker genes including *Timd4, Lyve1,* and classical alternatively-activated (M2-like) macrophage markers *Cd163* and *Mrc1*.[2,6,13,14] In the naïve mouse heart, CD206 (*Mrc1*)-expressing resident macrophages are primarily CCR2^{-} and express high levels of the markers *Ym1* and *Fizz1*.[15] After acute MI, CD206^{+} macrophages expand in the infarct and border zone (peaking at 7 d post-MI)[15,16] to promote wound healing and limit adverse remodeling.[15,17] CD206^{+} macrophages are activated by Th2 cytokines IL-4/13, and IL-10.[18-20] IL-4/13 are important inducers of a reparative and pro-fibrotic phenotype,[18,19,21] signaling through Type I or II IL-4 receptors containing the common alpha chain IL4Rα, resulting

in STAT6-mediated activation of *Arg1*, *Mrc1*, *Fizz1* (*Retnla*), *Ym1*, and secretion of C-C motif chemokine ligands (CCL)-17 and -22.[18,20,22,23] In vivo administration of IL-4 acutely after MI improves wound healing and remodeling via the modulation of $CD206^+$ macrophages. However, this beneficial effect is lost when IL-4 is given late after MI.[15,24]

These prior studies highlight $CD206^+$ macrophages as key mediators of the post-MI wound healing response. However, the importance of this macrophage population in the chronically failing heart, which exhibits a considerably different immune cell profile,[1,11] is unknown. In chronic ischemic cardiomyopathy, locally sourced and proliferating cardiac macrophages exhibit much greater *Mrc1* and *Fizz1* expression than monocyte-derived macrophages.[5] Moreover, in chronic pulmonary and renal disease, persistent M[IL-4/13] activation or M2-like macrophage recruitment can contribute to tissue fibrosis,[21,25] whereas we have previously shown that the post-MI failing heart exhibits increased IL-4/13 expression coincident with a Th2 $CD4^+$ T-cell profile.[26] Hence, here we tested the hypothesis that expansion of cardiac $CD206^+$ macrophages, activated by IL-4 receptor signaling, are key mediators of LV remodeling in chronic ischemic HF.

METHODS

Mouse models. All mouse studies complied with the National Research Council's Guide for the Care and Use of Laboratory Animals (revised 2011) and were locally approved by Institutional Animal Care and Use Committees at the University of Alabama at Birmingham and Washington University in St. Louis. CD45.2 (#000664) and CD45.1 (#002014) C57BL/6 mice, Fizz1$^{-/-}$ mice (#029976), and LysM-Cre^{ERT2} mice (#031674) were purchased from Jackson Laboratory. Floxed IL4Rα (IL4Rα$^{f/f}$) mice[27] were originally obtained from Dr. Frank Brombacher (University of Cape Town) and bred with LysM-Cre^{ERT2} mice to generate IL-4Rα$^{f/f}$LysM-Cre^{ERT2} mice that allow for tamoxifen-inducible myeloid-specific deletion of IL-4Rα. To induce Cre-mediated recombination, mice were fed tamoxifen citrate chow (40 mg/kg/d; Inotiv TD.130860).

As 400mg/kg tamoxifen citrate is sufficient to induce recombination,[28] IL-4Rα$^{f/f}$LysM-Cre^{ERT2} mice were considered to reach stable myeloid-specific IL4Rα deletion after 2 w of feeding. Male mice were used for experiments unless otherwise indicated. Mice were housed in temperature-controlled cages under a 12-hour light-dark cycle and given free access to water and regular chow. A total of 248 male and 37 female mice at 8-10 weeks of age were used. After terminal experiments, mice were euthanized by isoflurane inhalation (2%).

Murine surgical procedures. Permanent coronary ligation to induce large MI and ischemic HF, and control sham surgery, were performed under general anesthesia with 1-1.5% inhaled isoflurane and mechanical ventilation as previously described.[4,26,29-31] For macrophage adoptive transfer, cell suspensions ($1x10^6$ polarized macrophages in 50 μL sterile PBS) or sterile PBS control alone were injected intramyocardially into the free wall of left ventricle (10 μL/site x 5 sites) in naïve C57BL/6 male recipient mice.

Echocardiography. M-mode and 2-dimensional echocardiography were performed under 2% inhaled isoflurane anesthesia (with 98% O_2) and continuous ECG monitoring using a VisualSonics Vevo 3100 High-Resolution System and 30 MHz MX400 transducer with a heated, bench-mounted adjustable rail system.[4,26,29,32,33] Imaging was performed in the parasternal long-axis and short-axis views. LV chamber volume in end-diastole (EDV) and end-systole (ESV) were quantitated using the area-length method from long-axis images captured in ECG-gated Kilohertz Visualization mode. Systolic function was indexed by LV ejection fraction (EF), calculated as [(EDV−ESV)/EDV] * 100. Stroke volume was defined as EDV−ESV. LV mass (mg) was calculated as $1.05*[(IVSWTd+EDD+PWTd)^3-(EDD)^3]$, where IVSWTd and PWTd are interventricular septal and LV posterior wall thickness at end-diastole, and EDD is the LV end-diastolic diameter derived from M-mode tracings.

Gene expression analysis. Total RNA from LV remote zones (≈10 mg), macrophages and cMSCs was extracted using Trizol (Invitrogen, 15596026) and Qiagen RNAeasy Columns

(QIAGEN, 74204)[34] and reverse transcribed to cDNA using the High-Capacity cDNA Reverse Transcription Kit (Applied Biosystems, 43-688-14). cDNAs were subjected to qPCR using SYBR Green Master Mix (Applied Biosystems, A25742) and run on a ViiA 7 RT PCR System (Applied Biosystems).[32,35-37] Forward and reverse primer sequences are listed in *Supplemental Table 1*.

Multiplex Luminex assay. Peripheral blood was coagulated on ice and centrifuged to separate serum. Cytokine Luminex assay of serum samples was performed in 96-well Bio-Plex Pro Mouse Cytokine microplates and analyzed using the Luminex reader (BIO-RAD, Bio-PlexTM 200 system) according to the manufacturer's protocol.[34] Bio-Plex Pro Mouse Cytokine 23-plex Assay (M60009RDPD), MIP-2 Set (171G6006M), TGF-β1 Set (171V4001M), Standards Group I (171I50001), Group II Standards (171I60001), TGF-β Standard (171X40001) and Reagent Kit V (12002798) were all purchased from BIO-RAD.

Immunoblot analysis. Immunoblotting was conducted using standard protocols as described previously,[33,34,36] using antibodies against mouse Notch1 (Cell Signaling, 4380), NICD (Cell Signaling, 4147) and α-SMA (Abcam, ab7817). GAPDH (Cell Signaling, 97166) and α-tubulin (Santa Cruz, 5286) were used as loading controls.

Immune cell isolation and flow cytometry. Live mononuclear cells were isolated from peripheral blood and heart tissue and processed for flow cytometry as previously described.[26,29,38] After 1% paraformaldehyde fixation, isolated cells were resuspended in MACS buffer (PBS with 2 mM EDTA and 0.5% BSA) and preincubated for 10 min at 4°C with anti-mouse CD16/CD32 antibody (eBioscience, #14-0161-82) to block Fcγ receptors.[32] Cells were then stained for surface membrane markers upon incubation with fluorophore-labeled anti-mouse CD45, F4/80, MERTK, CD11b, Ly6G, Ly6C, CD3, CD4, CD8, IL-4Rα, IL-10Rα, MHCII, LYVE1, and CCR2, and, for human cardiac mononuclear cells, anti-human CD45, CD64, CD206 and CCR2 for 1 h. Mouse cardiac mononuclear cells were then permeabilized with 0.5% Tween-20 for 20 minutes, followed by staining with anti-mouse CD206 and Ki67 for 1 h. All

staining was performed on ice to maintain cell morphology. Flow cytometry was performed using a FACSdiva LSR-II flow cytometer (BD) and analyzed using FlowJo software v10.8.0. Specific details regarding the fluorophore-conjugated antibodies used are listed in *Supplemental Table 2*.

(Immuno)histological analysis. Formalin-fixed, paraffin-embedded heart tissues were sectioned at 5 μm thickness, deparaffinized, and rehydrated. Cardiomyocyte cell membranes and capillaries were stained using Alexa Fluor (AF)555-conjugated wheat-germ agglutinin (Invitrogen, #W32464) and AF488-conjugated isolectin-IB_4 (Invitrogen, #121411), respectively.[4,26,29,32]. After antigen retrieval, LV sections were stained with anti-mouse CD206 (1:50, R&D AF2535, secondary anti-goat AF555), Ki67 (1:50, eBioscience 14-5698-82, secondary anti-rat AF488), CD45.2 (1:50, eBioscience 14-0454-82, secondary anti-mouse AF647), α-actinin (1:100, Sigma A2172, secondary anti-mouse AF555), IL-4Rα (1:50, Invitrogen PA5-103142, secondary anti-rabbit AFF647) and FIZZ1 (1:50, R&D MAB-1523, secondary anti-rat AF488) or anti-human CD163 (1:100, Leica Biosystems CD163-L-CE, secondary anti-mouse IgG1 AF647), IL-4Rα (1:50, R&D MAB230, secondary anti-mouse IgG2a AF488) and FIZZ3 (1:50, R&D AF1359, secondary anti-goat AF555) antibodies. After permeabilization with 20 μg/ml proteinase K, α-actinin stained LV sections were incubated with TUNEL reaction mix (Biotium 30063) for 2h at 37°C. CD206 or CD163 stained LV sections were incubated with 15 μM heat-dissociated collagen hybridizing peptide 5-FAM Conjugate (F-CHP) (3Hekix FLU300) overnight at 4°C. In addition, LV frozen sections (8 μm) were fixed with acetone/chloroform, rehydrated, and stained with anti-mouse F4/80 (1:100, Abcam ab6640, secondary anti-rat AF488) and α-actinin (1:100, Sigma A2172, secondary anti-mouse AF555) antibodies. Nuclei were stained with DAPI. Images were acquired using a Nikon A1 confocal microscope. Fibrosis was measured in LV sections using Masson's Trichrome staining, and images were captured by a Nikon 80i Nomarski DIC microscope. Collagen (blue) staining percent of total cross-sectional

area was determined as previously described.[4,26,29,32] Staining was quantified from more than 5 high-power fields (40x) per section using Nikon NIS-Elements software, version 4.60.00.

Bone marrow macrophage culture and adoptive cell transfer. C57BL/6 (CD45.2) or *Fizz1*$^{-/-}$ mouse bone marrow (BM) cells were harvested aseptically and cultured in RPMI 1640 medium, supplemented with 10% fetal bovine serum (FBS), 1% penicillin-streptomycin (PS) and 30 ng/mL recombinant mouse macrophage-colony-stimulating factor (M-CSF, R&D, 416-ML) at 37°C. The supernatant was replaced with fresh complete medium containing 30 ng/mL M-CSF every 3 days for the attached cells, following the protocol of Trouplin et al.[39] After 7 days of differentiation, BM-derived macrophages (BMDMs) were cultured in RPMI 1640 with 10% FBS and 1% PS for 24 h for M0 (resting) macrophages, with 40 ng/mL recombinant mouse IL-4 (R&D, 404-ML) for M[IL-4] macrophages, and with 40 ng/mL recombinant mouse IL-10 (R&D, 417-ML) for M[IL-10] macrophages. Polarized macrophages were then mechanically detached, and cell aliquots were stained with anti-mouse CD45, F4/80 and CD206 (*Supplemental Table 2*) and analyzed using a flow cytometer to evaluate macrophage purity. After 24 h of polarization, M0, M[IL-4] and M[IL-10] cells were rinsed with PBS and cultured in FBS-free medium for 3 h. The macrophage conditioned medium was subsequently collected for treatment of cardiac mesenchymal stem cells and fibroblasts, as described below. The polarized macrophages were used for studies of intramyocardial adoptive cell transfer into naïve male CD45.1 C57BL/6 mice as described above.

***In vivo* antisense oligonucleotide administration.** Second-generation chimeric 20-base IL-4Rα antisense oligonucleotides (ASOs) (CCGCTGTTCTCAGGTGACAT) and control mismatched oligonucleotides (MM oligos) (CCGCTCATCACTGCTGACAT) were synthesized by Integrated DNA Technologies (IDT). All 20-base oligonucleotides were designed to avoid murine immune-stimulatory motifs, and contained phosphorothioate backbones and 2'-O-methoxyethylribose (MOE)-modification on bases 1–5 and 16–20 as described previously.[40,41] Oligonucleotides were suspended in sterile saline and administered every 3 days (40 mg/kg,

total volume 10 µL saline/g body weight) by intraperitoneal injection.[41] Male C57BL/6 sham-operated and HF mice (4 w post-MI) with comparable degrees of LV remodeling were randomized to receive either IL-4Rα ASOs (Ref 219428745, IDT) or MM oligos (Ref 219428746, IDT) for 4 w.

***In vivo* phagocytosis assay.** To assess cardiac macrophage phagocytosis *in vivo*, pHrodo™ green-E. coli bioparticles (Invitrogen, P35366) were injected intraperitoneally to mice (200 µg/mouse) 4 h before sacrifice. After sacrifice, heart mononuclear cells were collected and cell surface marker staining performed with anti-mouse CD45, F4/80, MERTK and CD206 as described above. Bioparticle uptake in live macrophages was measured by flow cytometry.

Cardiac mesenchymal stem cell (cMSC) studies *in vitro*. $Sca1^{+}CD90^{+}CD31^{-}DDR2^{-}$ cMSCs were isolated from mouse hearts and maintained in supplemented [DMEM]/Ham's F-12 culture medium as previously described,[33] and used within 3-5 cell passages for all experiments. For isolated cell stimulation studies, cMSCs were treated at the indicated times with serum-free conditioned RPMI 1640 medium from M0, M[IL-4], or M[IL-10] macrophages described above (or control media alone), with some experiments performed in the presence of either 1.5 µg/mL Fizz1 neutralization antibody or IgG isotype control (antibodies-online.com, ABIN636644 and ABIN1881001, respectively). In separate studies, cMSCs were treated with recombinant mouse Fizz1 (Leinco Technologies, R1140) at the indicated concentrations and times in serum-free RPMI 1640 medium.

Collagen gel-contraction assays. These were performed as previously described.[33] Briefly, cMSCs in ice-cold 10% FBS DMEM medium mixed with 1 mg/mL rat tail collagen I were plated in 48-well tissue culture plates at a density of $3x10^5$ cells/well. The cell suspension was incubated at 37°C for 30 minutes until gelation. After gel formation, an additional 0.5 mL of 10% FBS DMEM medium was added to each well and incubated overnight at 37°C in a 5% CO_2 incubator. The supernatant was then removed and the gels treated with 0.5 mL conditioned

RPMI 1640 medium from M0, M[IL-4], or M[IL-10] macrophages with 10% FBS (or media alone control), with or without anti-Fizz1 or IgG isotype control (1.5 μg/mL), as described above. Some experiments were performed upon incubation with IL-4 or IL-10 alone (40 ng/mL) in 10% FBS RPMI 1640 medium. The cells were cultured and treated for 5 d with medium change every 2 d. On day 5, the gels were detached from the wells using a pipette tip and incubated overnight. On day 6, the gels were imaged with a digital camera and gel area was measured using Image J software (1.51j8, NIH).

siRNA transfection of cMSCs. cMSCs were transfected with siRNA using INTERFERin Reagent (Polyplus, 101000028) according to the manufacturer's protocol. Control siRNA (4390843) and siRNA targeting Notch1 (4390771) were purchased from Invitrogen.

Cardiac fibroblast studies *in vitro*. Mouse cardiac fibroblasts were purchased from iXCells biotechnologies (10MU-015) and grown in fibroblast growth medium (MD-0011) at 37°C in a humidified 5% CO2 atmosphere. Cells were used within 1-3 passages and treated with M0, M[IL-4], or M[IL-10] conditioned medium for 24 h.

Human studies. Following patient consent, failing heart tissue was procured from patients with advanced (NYHA IV) HF with reduced EF undergoing LV assist device (LVAD) placement at the University of Alabama at Birmingham (UAB) under the auspices of Institutional Review Board (IRB) approved protocol #X090810003. Non-failing control heart tissues were obtained from donor hearts technically unsuitable for heart transplantation from the Alabama Organ Center. All protocols using human heart samples were approved by the UAB IRB. Failing and control human heart tissues were used for cardiac immune cell isolation and subsequent flow cytometry, as well for histological analysis. Clinical characteristics of human HF subjects and donor controls are shown in *Supplemental Table 3.*

Statistical Analysis. All group data are mean ± SD. All statistical analyses were performed with GraphPad Prism 9 (GraphPad Software). Normality was assessed using the Shapiro-Wilk test, whereas group variances were compared using the Brown-Forsythe test. For

normally distributed data, a two-tailed unpaired Student's *t* test with equal or unequal variance was used for two-group analyses, and 1- or 2-way ANOVA with Tukey's post-test was used for multi-group analyses. Additionally, 2-way repeated-measures ANOVA with Dunnett's multiple comparison test was used to analyze time series pre-post data. For non-normal distributions, the Mann-Whitney U test was used for 2-group analyses. Pearson R correlation test was used for linear dependence analyses. Specific approaches are in the figure legends. A *p* value of <0.05 was considered statistically significant.

RESULTS

Cardiac CD206$^+$ macrophages progressively expand during the development of chronic HF post-MI. Cardiac macrophage subsets were profiled using flow cytometry at various timepoints following non-reperfused large MI during the development of ischemic HF,[4,26,29,36] and in sham-operated controls (*Figure 1A*). As shown in *Figures 1B-C and S1A*, following MI there was significant cardiac accumulation of both overall CD45$^+$ leukocytes and total F4/80$^+$MERTK$^+$ macrophages in a biphasic manner, with high levels at 48 h after injury, subsequent decline by 2 w, followed by a second phase of re-expansion up to 8 w post-MI during chronic LV remodeling and failure. In the failing heart 8 w post-MI, macrophages comprised nearly two-thirds (~63%, or ~140,000 cells per heart) of all cardiac leukocytes and were increased by ~9-fold over macrophage levels in sham-operated hearts. Similar dynamics were observed for the blood levels of pro-inflammatory Ly6C^{high} monocytes, an important source of infiltrating macrophages,[3,5,10,32,42] during the progression of ischemic HF. No significant differences were observed in the levels of patrolling Ly6C^{low} monocytes between sham-operated and HF mice at any time point evaluated (*Figures S2A-C*).

We next further evaluated macrophage subsets in the mouse heart. Naïve murine hearts harbored low numbers of macrophages (~20,000/heart), of which ~90% expressed the resident macrophage marker CD206 (*Figure 1C*). However, acutely (48 h) after MI, CD206$^+$ macrophages comprised only ~20% of overall macrophages in the heart, in the setting of a

marked expansion of CD206$^-$ macrophages early after MI. Thereafter, both the frequency and absolute number of CD206$^+$ macrophages steadily increased in post-MI hearts during the progression of LV remodeling, such that at 8 w post-MI ~85% of cardiac macrophages expressed CD206. In contrast, CD206$^-$ macrophage levels decreased markedly by 2 w post-MI, and then exhibited smaller sustained increases in chronically failing hearts thereafter. Both populations were significantly increased as compared to sham-operated hearts at all timepoints post-MI. Hence, macrophages expand significantly in the chronically remodeled and failing heart post-MI, and most of these macrophages express CD206.

Cardiac CD206$^+$ macrophages robustly express IL-4Rα in chronic HF. Two key activators of CD206$^+$ macrophages are IL-4/13, acting via Type I or II IL-4 receptors (IL-4R) containing the common subunit IL4Rα,[43-45] and IL-10, signaling through the IL-10 receptor (IL-10R) complex upon binding to the high affinity IL-10Rα (IL-R1) subunit.[46,47] As illustrated in *Figure 1D*, both CD206$^+$IL4Rα$^+$ and CD206$^+$IL-10Rα$^+$ macrophage subpopulations were significantly increased in comparison to sham-operated hearts at all time points after MI. However, there was substantial expansion of the CD206$^+$IL4Rα$^+$ population over time, such that at 8 w post-MI, levels of CD206$^+$IL-4Rα$^+$ cells (~45,000 per heart) were ~8-fold higher than CD206$^+$IL-10Rα$^+$ cells and comprised ~42% of all CD206$^+$ macrophages in the chronically failing heart. In contrast, at 1 w post-MI, during the healing phase, CD206$^+$IL-10Rα$^+$ macrophages were more abundant than CD206$^+$IL-4Rα$^+$ cells, comprising ~40% of all CD206$^+$ macrophages in the heart. Notably, neither IL-4Rα nor IL-10Rα were abundantly expressed by cardiac CD206$^-$ macrophages (<3% of cells) at any timepoint post-MI, and CD206$^-$ macrophages expressing either IL-4Rα or IL-10Rα numbered fewer than 500 cells/heart in the chronic stages of LV remodeling (*Figure S1B*). In addition, IL-4Rα and IL-10Rα expression was also very low in blood neutrophils (<1.5%), Ly6C^{low} monocytes (<2%) and Ly6C^{high} monocytes (<5%) in both sham and HF mice (*Figure S2*).

Regarding Th2 cytokines, serum levels of IL4 and IL-10 were significantly higher in MI mice as compared with sham mice during both the healing phase (1 w) and chronic remodeling phase (8 w) post-MI, whereas levels of IL-13 and TGF-β1 were comparable in sham and MI mice at all timepoints (*Figure S3A*). In contrast, serum levels of the pro-inflammatory cytokines TNF-α, IFN-γ, IL-1β, MCP-1 and MIP-2α in HF mice were increased over sham controls during both the early and late phases of remodeling after MI (*Figure S3B*), consistent with ongoing systemic inflammation in HF mice. Hence, $CD206^+$ macrophages in the failing heart primarily express IL-4Rα (versus IL-10Rα); this is accompanied by increased circulating levels of both IL-4 and IL-10.

$CD206^+$ macrophages in the failing heart proliferate, are primarily $CCR2^-$, $MHCII^{hi}$, and $LYVE1^+$ and correlate with LV dysfunction and fibrosis. At 8 w post-MI, HF mice exhibited significant LV systolic dysfunction and fibrosis (*Figure 2A and S4A*). Cardiac $CD206^+$ macrophage abundance inversely correlated with LVEF (r = 0.695), and directly correlated with border and remote zone fibrosis (r = 0.755 and 0.644, respectively). Tissue co-staining with anti-CD206 and fluorescein-conjugated collagen hybridizing peptide (CHP) that recognizes denatured collagen[48] revealed that $CD206^+$ macrophages were primarily found in areas of collagen turnover in the failing heart, with >98% of macrophages associated with CHP-positive regions in the infarct and border zones, and >80% CHP-associated cells in the remote myocardium (*Figure 2B*). To infer the source of $CD206^+$ macrophage expansion in the failing heart, we measured the expression of markers CCR2, MHCII, and LYVE1 by flow cytometry (*Figure 2C*). In sham hearts, >90% $CD206^+$ macrophages were $CCR2^-$, and of these, ~95% were $LYVE\text{-}1^+$, indicating a primarily resident macrophage population. In failing hearts, the proportion of $CD206^+CCR2^-LYVE1^+$ macrophages decreased significantly but remained high at ~80% of total $CD206^+$ cells, suggesting resident cell predominance but with an increased

contribution from monocyte-derived macrophages. Moreover, in both sham and failing hearts, the majority (~70%) of $CD206^+$ macrophages were $MHCII^{hi}$.

Resident macrophage expansion requires local cell proliferation. As shown in *Figure 2D and S4B*, immunostaining for CD206 and the cell proliferation marker Ki67 revealed that both total $CD206^+$ and $Ki67^+CD206^+$ macrophages were robustly expanded in the failing heart (8 w post-MI) as compared to sham. Cell density was greatest in the infarct zone (855 cells/mm^2; 9% $Ki67^+$), followed by the border zone (584 cells/mm^2; ~8% $Ki67^+$) and then the remote zone (290 cells/mm^2, Ki67 positivity ~3% similar to sham hearts). Complementary assessment using flow cytometry demonstrated that in both sham and failing hearts only $CD206^+$ macrophages exhibited Ki67 positivity (*Figure 2E*). Moreover, as compared to sham, failing hearts evidenced ~3-fold higher levels of $CD206^+Ki67^+$ macrophages (~10% total), confirming augmented local proliferation of $CD206^+$ macrophages. In parallel, myocardial gene expression of Th2 cytokines IL-4 and IL-10 (but not IL-13) and classical alternatively-activated macrophage markers *Mrc1 (CD206), Arg1, Ym1* and *Fizz1* was significantly increased in failing versus sham hearts (*Figure S4C*), Concomitantly, the expression of fibrotic genes *(Col)1α1, Col1α2*, and *Col3α1* was markedly increased in failing hearts. Collectively, these data support expansion of a Th2/M2-like immuno-fibrotic response in the chronically failing heart post-MI.

IL-4 polarization *in vitro* induces a profibrotic phenotype in $CD206^+$ macrophages. Bone marrow-derived macrophages (BMDMs) were polarized with either IL-4 or IL-10 (40ng/mL), or medium alone (M0 control), for 24 h (*Figure 3A*). Flow cytometry indicated that while BMDMs were primarily $CD206^+$ under resting (M0) conditions, both IL-4 and Il-10 exposure augmented BMDM CD206 expression to ~98-99% of total cells. As shown in *Figure 3B*, the expression of signature M2 genes[15,18,20,49,50] *Mrc1, Arg1*, and *Ym1* significantly increased in both M[IL-4] and M[IL-10] macrophages (with much more *Arg1* and *Ym1* expression in M[IL-4] cells) as compared to non-polarized M0 macrophages. In contrast, expression of *Fizz1* (found in inflammatory zone 1), a protein secreted during Th2 responses[51,52] and implicated in

myofibroblast differentiation and lung fibrosis,[53,54] only increased in M[IL-4] macrophages, and to extraordinary levels (>7,500-fold). Conversely, *B7-H4* was exclusively, albeit modestly, upregulated in M[IL-10] macrophages. Changes in macrophage gene expression were noted after 4 h of polarization (*Figure S5A*) and were maintained or augmented after 48 h (*Figure S5B*). A range of responses was observed for inflammatory and repair-associated genes in BMDMs after 24 h of polarization *in vitro* (*Figure S6A*). Surprisingly, there was no upregulation of profibrotic genes TGF-β1 and platelet-derived growth factor (PDGF)-BB in M[IL-4] and M[IL10] macrophages as compared to M0 cells, although there was augmented expression of tissue inhibitor of matrix metalloproteinase (TIMP)-1 and TIMP-3 in both M[IL-4] and M[IL-10] macrophages.

In parallel experiments, conditioned medium was collected from M0, M[IL-4] and M[IL-10] macrophages and applied to $Sca1^{+}CD90^{+}CD31^{-}DDR2^{-}$ cardiac MSCs[33] (*Figure 3A*). cMSC gene expression was then evaluated after 6 and 16 h of exposure. Short-term (6 h) exposure to M[IL-4] medium induced significant upregulation of the proliferation genes *PCNA*, *Mki67, CyclinB1* and *CyclinD1* as compared to M0-medium, and to a greater extent than upon exposure to M[IL-10] medium. Longer-term (16 h) exposure induced similar expression responses for cMSC pro-fibrotic genes, including α-smooth muscle actin *(α-SMA*), *Col1α1, Col1α2*, and *Col3α1* (*Figure 3C*). The functional impact of macrophage polarization on cMSCs was assessed using collagen gel contraction assays[33] after 5 d of exposure to M0, M[IL-4], M[IL-10] medium, or medium alone control. As illustrated in *Figure 3D*, M[IL-4] medium exposure induced robust gel contraction, significantly greater than with exposure to either M0 or M[IL-10] medium (or control), consistent with vigorous cMSC myofibroblast differentiation. Importantly, exposure to complete medium containing IL-4 or IL-10 alone (40 ng/mL) did not induce cMSC gel contraction (*Figure S6B*), indicating an indispensable role for $CD206^{+}$ macrophages in IL-4-induced cMSC myofibroblast differentiation. Similarly, 24 h treatment with

M[1L-4] medium robustly increased α-SMA protein expression in mouse cardiac fibroblasts as compared with similar treatment with M0 or M[IL-10] medium (*Figure S6C*). Collectively, these data suggest that IL-4-mediated macrophage polarization supports pro-fibrotic responses in concert with striking upregulation of *Fizz1*.

Adoptive transfer of M[IL-4] macrophages to naïve hearts induces cardiac dysfunction and fibrosis. To evaluate the in vivo cardiac effects of M[IL-4] and M[IL-10] macrophages, we adoptively transferred $1x10^6$ M0, M[IL-4], or M[IL-10] bone marrow-derived macrophages from CD45.2 male mice to naïve WT CD45.1 male mice (PBS control) via intramyocardial injection, with subsequent follow-up over 4 w (*Figure 4A*). Immunostaining of injection sites of recipient hearts 30 minutes post-injection confirmed successful transfer of M0, M[IL-4], and M[IL-10] donor macrophages (*Figure S7A*). Serial echocardiography of recipient mice revealed progressive and significant LV chamber dilatation, with increased EDV and ESV, and systolic dysfunction, with reduced LVEF, along with LV hypertrophy, evidenced by increased LV mass, IVSWTd, and PWTd by echocardiography and increased normalized heart weight, in M[IL-4] macrophage recipients, but not in PBS, or M0 or M[IL-10] macrophage recipients (*Figures 4B and S7B and D*). Stroke volume was comparable over time in all four groups (*Figure S7C*). Histological analysis showed significantly increased patchy interstitial fibrosis in M[IL-4]-recipient hearts as compared with PBS, M0, and M[IL-10] recipient hearts (*Figure 4C*), along with augmented cardiomyocyte cross-sectional area and apoptosis (*Figures 4D and S7E*). Importantly, CD45.2 and CD206 co-staining of recipient hearts demonstrated donor macrophage persistence in adoptive transfer recipients, but to a significantly greater level in M[IL-4] recipient mice. M[IL-4] (but not M0 or M[IL-10]) macrophage transfer also induced expansion of native resident $CD206^+$ macrophages. Both $CD45.2^+$ donor and $CD45.2^-$ recipient $CD206^+$ macrophages expansion occurred primarily at sites of collagen turnover and fibrosis in recipient hearts, with stronger such association for donor macrophages (*Figures 4E and S7F*),

There was no evidence of pro-inflammatory Ly6C^{hi} monocytosis in any recipient mouse group (*Figure S7G*), suggesting the absence of systemic inflammation after transfer. Collectively, these data establish that M[IL-4] polarized macrophages are sufficient to induce chronic cardiac remodeling, hypertrophy, and fibrosis, and a microenvironment supporting CD206^{+} macrophage expansion.

Myeloid-specific IL-4Rα deletion in HF suppresses cardiac CD206^{+} macrophage expansion and improves LV remodeling. Among myeloid cells, IL-4Rα expressions occurred primarily in macrophages, with low levels in monocytes and neutrophils (*Figure S2*), and among macrophages, primarily in CD206^{+} macrophages (*Figures 1D and S1B*). Hence, to establish the role of CD206^{+}IL4Rα^{+} macrophages in HF, we used IL-4Rα$^{f/f}$LysM-Cre^{ERT2} mice. Given the importance of the IL-4 axis in wound healing after acute MI[15,24] and our observations that cardiac CD206^{+}IL-4Rα^{+} macrophage expansion in ischemic HF occurs most prominently ≥4 w post-MI, we induced myeloid IL-4Rα deletion during late remodeling. Male and female IL-4Rα$^{f/f}$ and IL-4Rα$^{f/f}$LysM-Cre^{ERT2} HF mice with comparable LV remodeling at 4 w post-MI (or sham-operated controls) were randomized to receive tamoxifen diet for 6 weeks (*Figure 5A*). In male mice, echocardiography revealed significant LV dilation and systolic dysfunction in both HF groups 4 w post-MI as compared to sham (*Figure 5B*). In contrast, as compared with tamoxifen-fed IL-4Rα$^{f/f}$ HF mice, tamoxifen treatment for 6 w in IL-4Rα$^{f/f}$LysM-Cre^{ERT2} HF mice resulted in lower LVEDV and ESV, better LVEF and stroke volume (SV), and smaller heart size and normalized heart and lung weight (*Figures 5B, S8A-B*). Moreover, histological analysis revealed less border and remote zone fibrosis, smaller cardiomyocyte area, and improved capillary density in male IL-4Rα$^{f/f}$LysM-Cre^{ERT2} HF mice versus IL-4Rα$^{f/f}$ HF mice (*Figures 5C, S8C*). Myeloid IL-4Rα deletion in HF in male mice also decreased levels of total leukocytes, CD206^{+} and CD206^{-} (and CD206^{-}IL4Rα^{+}) macrophages, CD206^{+}IL4Rα^{+} and CD206^{+}IL10Rα^{+} macrophages, and proliferating Ki67^{+}CD206^{+} macrophages in the heart, as well as Ly6C^{hi} and

Ly6C^{hi}IL-4Rα^{+} monocytes (but not Ly6C^{low} monocytes) in the blood, as compared to HF mice without myeloid IL-4Rα deletion (*Figures 5D-F, S8D-F*). There were no effects of myeloid IL-4Rα deletion on any parameter in sham male mice.

Comparable tamoxifen-induced effects were observed in female IL-4Rα$^{f/f}$LysM-Cre^{ERT2} versus IL-4Rα$^{f/f}$ HF mice with regard to improvements in LV remodeling and systolic function (albeit with less pronounced differences in LVEDV) (*Figure S9A-B*), heart and lung gravimetry and weight (*Figure S9C-D*), and reductions in cardiac leukocytes and total macrophages (Figure S10A), CD206^{+} and CD206^{-} macrophages, CD206^{+}IL4Rα^{+} and CD206^{+}IL10Rα^{+} macrophages, and CD206^{-}IL4Rα^{+} macrophages (*Figures S10B-C*). As in males no effects of myeloid IL-4Rα deletion on any of these parameters were observed in sham-operated female mice. Collectively, these results indicate that CD206^{+}IL4Rα^{+} macrophages are a key expanded myeloid cell population in the failing heart that is necessary for driving progressive inflammation and pathological cardiac remodeling, fibrosis, and dysfunction. Moreover, IL-4Rα expression marks a macrophage subpopulation with high proliferative capacity in the failing heart.

IL-4Rα silencing *in vivo* reverses LV remodeling, reduces cardiac fibrosis, and improves neovascularization in HF. To explore whether the macrophage IL-4Rα axis could be exploited for therapeutic benefit in HF, we selectively silenced IL-4Rα expression *in vivo* using optimized antisense oligonucleotides (ASOs) targeting IL-4Rα mRNA.[40,41] IL-4Rα signaling mainly occurs in hematopoietic and lymphoid cells.[45] In humans, there is very low IL-4R RNA expression in heart cardiomyocytes and fibroblasts, with much more pronounced expression in immune cells, and in endothelial and smooth muscle cells (https://www.proteinatlas.org/ENSG00000077238-IL4R/single+cell+type/heart+muscle). To assure targeting of cardiac macrophages with this systemic approach, we performed flow cytometry to evaluate IL-4Rα expression in cardiac leukocytes. As shown in *Figure S11*, in both sham and failing hearts, ~92% of all IL-4Rα^{+} CD45^{+} leukocytes were macrophages

(F4/80$^+$MERTK$^+$), while ~98% of IL-4Rα$^+$ macrophages in failing hearts were CD206$^+$. Moreover, circulating monocytes and neutrophils exhibited low levels of IL-4Rα expression (*Figure S2*). Hence, IL-4Rα ASOs represent a feasible and directed approach for dual inhibition of IL-4 and IL-13 signaling[45] in cardiac CD206$^+$IL-4Rα$^+$ macrophages.

Male sham-operated and HF mice with comparable degrees of LV remodeling at 4 w post-MI were randomized to receive either IL-4Rα ASOs or MM oligos (40 mg/kg every 3 days) for 4 weeks (*Figure 6A*). Body weight was comparable between the two sham groups and two HF groups over the 4 w treatment period (*Figure S12A*). Serial echocardiography revealed significant and expected LV dilation and systolic dysfunction in both HF groups as compared to sham groups (*Figures 6B and S12B*). Sham-operated mice exhibited no changes in LVEDV, LVESV, stroke volume (SV), and LVEF during treatment with either IL-4Rα ASOs or MM oligos. HF mice treated with MM oligos evidence progressive increases in LV chamber size, and reductions in LVEF and SV, over 4 w. In contrast, HF-IL-4Rα ASO mice, which exhibited LV remodeling similar to HF-MM oligo mice at 4 w post-MI, exhibited significant reductions in EDV and ESV, and improvements in SV and EF, indicative of reverse remodeling. Lung and heart gravimetric analysis at 8 w post MI revealed substantially attenuated pulmonary edema and cardiac hypertrophy in HF-IL-4Rα ASO HF mice versus HF-MM oligo mice, without impact on spleen weight (*Figures 6C and S12C*).

Histological evaluation with trichrome staining indicated significantly increased border and remote zone interstitial fibrosis in MM oligo-treated failing hearts as compared to MM oligo-treated sham hearts (*Figure 6D*). Impressively, IL-4Rα ASO treatment profoundly decreased both border and remote zone fibrosis in failing hearts. Fibrotic area in IL-4Rα ASO-treated sham hearts was comparable to that of MM oligo-treated sham hearts. Isolectin B4 and wheat-germ agglutinin staining (*Figure 6E*) indicated that both HF-MM oligo mice and HF-IL-4Rα ASO mice exhibited significantly increased myocyte cross-sectional area and lower myocardial

capillary:myocyte ratio versus their respective sham groups. Importantly, however, myocyte area was lower and capillary:myocyte ratio was higher in HF-IL-4Rα ASO mice versus HF-MM oligo mice, indicating alleviation of pathological hypertrophy and capillary rarefaction.

IL-4Rα silencing in HF depletes cardiac CD206$^+$IL-4Rα$^+$ macrophages and suppresses their proliferative and phagocytic capacity. As shown in *Figures S13A and 6F*, 4 w of IL-4Rα ASO treatment significantly reduced the number of total CD45$^+$ leukocytes (by ~45%), total F4/80$^+$MERTK$^+$ macrophages (by~53%), and both CD206$^+$ and CD206$^-$ macrophages (by ~50%) in the failing heart. Moreover, IL-4Rα ASO treatment specifically and profoundly depleted CD206$^+$IL-4Rα$^+$ cardiac macrophages, while mildly augmenting CD206$^+$IL-10Rα$^+$ macrophages in the failing heart (*Figure 6F*). IL-4Rα ASO administration did not impact leukocyte and total macrophage abundance in sham hearts. Notably, IL-4Rα ASO therapy did not impact in circulating IL-4 levels (nor IL-13 and TGF-β1 levels) in HF mice, whereas serum IL-10 was significantly decreased (*Figures 6G and S13B*). Remarkably, total CD206$^-$ macrophages, including CD206$^-$IL-4Rα$^+$ and CD206$^-$IL-10Rα$^+$ macrophages, in failing hearts were also diminished by IL-4Rα ASO treatment (*Figure S13A*). Additionally, IL-4Rα ASO treatment impacted CD206$^+$ macrophage function in failing hearts, significantly reducing (by ~50%) both CD206$^+$ macrophage cell proliferation (Ki67 staining) and phagocytic capacity (assessed in vivo using fluorescent bioparticles) in HF-IL-4Rα ASO mice as compared with HF-MM oligo mice (*Figures 6H-I*). The latter data are consistent with IL-4 serving as a potent stimulator of macrophage proliferation.[15,55]

IL-4Rα ASO treatment in HF mice also abrogated systemic inflammation as evidenced by normalization of circulating Ly6C^{hi} monocytosis (and levels of Ly6C^{hi}IL-4Rα$^+$ monocytes) and serum levels of pro-inflammatory protein mediators TNF-α, MCP-1, MIP-2α and IL-1β toward those observed in sham mice (*Figure S13C-D*). Serum IFN-γ levels, however, were not impacted by IL-4Rα ASO treatment and remained high in HF-IL-4Rα ASO mice as compared to

sham. Importantly, IL-4Rα ASO treatment in HF mice also alleviated T-cell expansion in both the circulation and failing heart, with significant reductions in peripheral blood and cardiac $CD4^+$ and $CD8^+$ T cells in in HF-IL-4Rα ASO mice as compared with HF-MM oligo mice (*Figure S14*). Additionally, IL-4Rα expression was very low (~1-2%) in blood and heart $CD4^+$ and $CD8^+$ T cells in both sham and HF mice treated with MM oligo or IL-4Rα ASOs. Taken together, these data indicate that in vivo IL-4Rα mRNA silencing was highly effective in improving pathological cardiac remodeling, hypertrophy, fibrosis, and dysfunction, and in suppressing local and systemic inflammation in chronic ischemic HF.

Fizz1 is essential for $CD206^+$ macrophage-induced myofibroblast activation. FIZZ1, also known as resistin-like molecule α (*Retnla*), is a 9.4 kDa cysteine-rich secreted protein produced mostly by macrophages during Th2 responses.[50-52] As described above, macrophage Fizz1 expression exponentially increased exclusively after M[IL-4] polarization (>7,500-fold after 24 h and >100,000-fold after 48 h) polarization and not with M[IL-10] polarization (*Figures 3B and S5B*), and coincided with M[IL-4] macrophage-induced myofibroblast differentiation of cMSCs (*Figure 3C*). Accordingly, we further evaluated the role of Fizz1 in pro-fibrotic cellular responses. Exposure of cultured cMSCs to recombinant mouse (rm) Fizz1 induced, in a dose-dependent manner, the expression of proliferative genes *PCNA, Mki67, CyclinB1* and *CyclinD1* early (2 h), and profibrotic genes *α-SMA, Col1α1, Col1α2*, and *Col3α1* late (16 h), after treatment (*Figure S15*), analogous to changes observed with M[IL-4] medium treatment (*Figure 3C*). To determine the need for FIZZ1 in M[IL-4]-induced cMSC responses, we used anti-Fizz1 antibody to neutralize endogenous Fizz1 in M[IL-4] conditioned medium. As shown in *Figure S16*, compared to IgG control, anti-Fizz1 significantly reduced the expression of mitotic genes, *α-SMA* (by 40%) and *Col3α1* in M[IL-4] conditioned media-treated cMSCs. Furthermore, anti-Fizz1 abrogated collagen gel contraction induced by M[IL-4] conditioned media (*Figure 7A*), a

phenomenon recapitulated by the use of Fizz1$^{-/-}$ BMDMs (*Figure 7B),* indicating that secreted Fizz1 is essential for M[IL-4]-induced cMSC myofibroblast differentiation and activation.

Notch signaling is critical for cell proliferation, differentiation, and development, and homeostasis;[56] Notch ligand binding to Notch receptors leads to release of Notch intracellular domain (NICD) and subsequent transcription of target genes, including *α-SMA, Cyclin D1, Cyclin A* and NF-κB.[56] As α-SMA expression is critical for myofibroblast fate of mesenchymal stromal cells,[33,57], we assessed the importance of Notch signaling in Fizz1-mediated α-SMA expression in cMSCs. Fizz1 exposure significantly upregulated cMSC gene expression of the Notch1 ligands DLL-4 and Jagged1 within 30 minutes (*Figure 7C*), followed by increased protein expression of Notch1, NICD and α-SMA within 24 h (*Figure 7D*). Importantly, Notch1 siRNA knockdown prevented α-SMA (and NICD) upregulation in Fizz1-treated cMSCs, suggesting a critical role for DLL-4/Jagged-Notch1 signaling in the pro-fibrotic effects of M[IL-4] macrophage-secreted FIZZ1.

In view of the importance of FIZZ1 in M[IL-4]-induced myofibroblast differentiation, we next examined Fizz1 expression and spatial distribution using immunostaining in failing hearts from MM oligo- and IL-4Rα ASO-treated mice (8 w post-MI). Consistent with flow data, a robust (~11-fold) expansion of CD206$^+$ macrophages (both IL-4Rα$^+$ and IL-4Rα$^-$) was observed in MM oligo-treated failing hearts versus sham hearts, especially in the border zone (*Figure 7E*). IL-4Rα staining was observed near exclusively in CD206$^+$ cells (*Figure S17*), further supporting CD206$^+$ macrophage-specificity of IL-4Rα silencing, and Fizz1$^+$ staining was near exclusively spatially localized to IL-4Rα$^+$ cells (~98% Fizz1$^+$) in all groups (*Figure S17*). IL-4Rα$^+$ Fizz1$^+$ cells comprised ~50% cardiac CD206$^+$ macrophages in HF-MM oligo mice (*Figure 7E*). IL-4Rα ASO treatment significantly decreased IL-4Rα$^+$Fizz1$^+$ (and IL-4Rα$^-$Fizz1$^-$) CD206$^+$ macrophages in failing hearts, and also diminished IL-4Rα expression (assessed by fluorescence intensity) (*Figure 7E*). (*Figures 7E and Figure S17*). Hence, IL-4Rα silencing in HF reduced CD206$^+$

macrophage FIZZ1 expression in the failing heart concomitantly with improvements in cardiac fibrosis. Taken together with the *in vitro* studies above, our results suggest that *Fizz1* may be a key contributor to the tissue level pro-fibrotic effects of $CD206^{+}IL\text{-}4R\alpha^{+}$ macrophages in the failing heart.

$IL\text{-}4R\alpha^{+}Fizz3^{+}$ alternatively activated macrophages expand and directly correlate with fibrosis in human failing hearts. To understand translational relevance, we lastly explored whether alternatively activated resident macrophages are expanded in human HF. As mentioned above, resident cardiac macrophages express classical M2-like markers *Mrc1* (*CD206*) and *CD163*.[2,6,13,14] Cardiac mononuclear cells were isolated from the LV apex procured from advanced HF patients during LVAD implantation, and from control donor hearts unsuitable for transplantation. Analogous to murine HF, flow cytometry indicated significant expansion (~10-fold) of $CD206^{+}$ macrophages ($CD45^{+}Autofluorescence^{+}CD64^{+}$) in human failing hearts versus control, with ~20% of $CD206^{+}$ macrophages expressing CCR2 (*Figure 8A*)**.** Human failing hearts also exhibited substantial (>200-fold) interstitial fibrosis versus control hearts, with most (~95%) $CD163^{+}$ macrophages found in association with areas of collagen turnover (*Figure 8B*), analogous to murine failing hearts. *Fizz3* (resistin, *Retn*), the human homolog of murine *Fizz1,* is expressed by M[IL-4/13] human macrophages and resembles mouse FIZZ1 with respect to sequence and function.[58,59] Accordingly, we performed immunostaining for IL-4Rα, Fizz3 and CD163, a widely used marker for alternatively-activated human macrophages.[60] As shown in *Figure 8C*, human failing hearts exhibited significant expansion (~6-fold) of $CD163^{+}$ macrophages (both $IL\text{-}4R\alpha^{+}$ and $IL\text{-}4R\alpha^{-}$) as compared to control hearts. $Fizz3^{+}$ staining was near exclusively spatially localized to $IL\text{-}4R\alpha^{+}$ cells (~98% $Fizz3^{+}$) in both human control and failing hearts, similar to the IL-4Rα and Fizz1 expression pattern observed in mouse hearts (*Figure S17*). Importantly, $IL\text{-}4R\alpha^{+}Fizz3^{+}$ cells comprised the predominant $CD163^{+}$ macrophage subset in human failing hearts, with approximately two-thirds of $CD163^{+}$ macrophages

583 expressing IL-4Rα and Fizz3^{+} (*Figure 8C*). CD163^{+} macrophage abundance directly correlated
584 with cardiac fibrosis in human HF. Hence, analogous to murine HF, human failing hearts also
585 evidence expansion of alternatively activated macrophages, likely with augmented IL-4 signaling
586 and contributing to pro-fibrotic responses.

587 **DISCUSSION**

588 We describe a novel role for cardiac CD206^{+} macrophages alternatively activated by IL-
589 4 receptor signaling in the progression of LV remodeling in ischemic cardiomyopathy. There are
590 several key findings. First, macrophages expressing CD206 comprised most macrophages in
591 the naïve heart. Following MI, cardiac CD206^{+} macrophages progressively expanded, especially
592 during the later stages of LV remodeling such that they comprised the predominant macrophage
593 population in chronic HF. Second, CD206^{+} macrophages were exclusively proliferative and
594 primarily CCR2^{-}, MHCII^{hi}, and LYVE1^{+} suggesting a resident cell population, and correlated with
595 LV dysfunction and fibrosis. Second, a sizable subpopulation of these macrophages in HF
596 expressed IL-4Rα; this occurred with attendant increased systemic levels of IL-4. Third, M[IL-4]
597 (but not M[IL-10]) CD206^{+} BMDMs induced remarkable upregulation of *Fizz1,* and robust cMSC
598 myofibroblast differentiation. M[IL-4] CD206^{+} macrophage-induced myofibroblast differentiation
599 and activation were dependent on FIZZ1 secretion and mediated in part by FIZZ1 induction of
600 DLL-4/Jagged1-Notch1 signaling in cMSCs. Fourth, intramyocardial adoptive transfer of M[IL-4]
601 macrophages was sufficient to induce pathological cardiac remodeling and fibrosis. Fifth,
602 myeloid-specific IL-4Rα deletion tempered cardiac CD206^{+} macrophage proliferation and
603 alleviated LV dysfunction, fibrosis, and adverse remodeling. Sixth, IL-4Rα silencing *in vivo* was
604 highly effective in depleting CD206^{+}IL-4Rα^{+} macrophages, reducing FIZZ1 expression in the
605 failing heart, and reversing LV remodeling in mice with established HF. Lastly, humans exhibit
606 expansion of alternatively activated macrophages in the failing heart marked by CD206 and
607 CD163 expression, with predominance of a subpopulation expressing IL-4Rα and Fizz3, the

608 human homolog of *Fizz1*. Collectively, these data establish that an expanded pool of
609 alternatively activated CD206^{+}IL-4Rα^{+} cardiac macrophages are key drivers of LV remodeling in
610 HF, inducing a Th2/M2-like immuno-fibrotic response in part dependent on FIZZ1. Targeting IL-
611 4 signaling in CD206^{+} macrophages may represent a fruitful therapeutic approach to limit long-
612 term cardiac remodeling in HF.

613 *Mrc1* (*Cd206*) and *Cd163* are typically expressed by resident cardiac macrophages
614 under steady state conditions.[2,6,13,14] Moreover, in the naïve heart, CD206^{+} macrophages
615 express high levels of classical M2-like genes such as *Ym1* and *Fizz1* and are primarily CCR2^{-}
616 ,[15] suggesting a macrophage subset with minimal monocyte-dependence.[6] Prior work has
617 shown that CD206^{+} macrophages expand during the first week after acute MI in the infarct and
618 border zone to promote infarct repair and functional restoration.[15-17] Administration of IL-4
619 acutely (but not late) after MI also expands CD206^{+} macrophages in the infarcted heart and
620 recapitulates beneficial effects on post-MI cardiac healing.[15,24] However, the role of this
621 macrophage population, and the impact of macrophage IL-4 signaling, in chronic LV remodeling
622 and ischemic HF has not been defined. The chronically failing heart is typically marked by
623 excessive tissue fibrosis.[61] Notably, in chronic pulmonary,[62,63] hepatic,[41] and renal[25] disease
624 models marked by excessive fibrosis, alternatively activated (CD206^{+} or CD163^{+}) macrophage
625 activation mediated by Th2 cytokines such as IL-4 contribute to disease progression. While we
626 have previously shown that the post-MI failing heart exhibits increased IL-4 expression and a
627 predominant Th2 CD4^{+} T-cell profile,[26] whether a similar pathophysiological axis contributes to
628 LV remodeling in ischemic cardiomyopathy is unknown.

629 Our studies show that CD206^{+} macrophages progressively expand after MI, with
630 particularly robust levels during the later stages of LV remodeling. Beyond the initial infiltration
631 of predominantly (>80%) CD206^{-} macrophages into the heart early (48 h) after MI, CD206^{+}
632 macrophages were the main subtype in the remodeling heart at 1 w post-MI and beyond,

comprising ~85% of all macrophages in HF. Moreover, in the failing heart 8 w post-MI, nearly half of all cardiac CD206$^+$ macrophages expressed IL-4Rα. Notably, cardiac macrophage proliferation was observed exclusively in CD206$^+$ subpopulation in the failing heart. Although spatially expanded throughout the myocardium, CD206$^+$ macrophages were most abundant in the infarct scar and border zone, and primarily in regions of collagen turnover and fibrosis. Heightened macrophage proliferation was also mainly seen in the scar and border zones. This suggests that progressive CD206$^+$ macrophage expansion in these regions may contribute to extracellular matrix remodeling, infarct expansion and LV chamber dilatation over time. Human HF also evidenced marked expansion of alternatively activated (CD206$^+$ or CD163$^+$) cardiac macrophages (consistent with a prior study of macrophages isolated from human failing hearts[64]) in association with regions of collagen denaturation and turnover, with a predominance of cells expressing IL-4Rα analogous to murine HF. In this regard, IL-4 is a known stimulator of tissue macrophage proliferation and resident macrophage self-renewal[55,65] that also augments macrophage CD206 expression[66] and promotes M2-like cardiac macrophage differentiation.[15] Consistent with our prior studies,[26] IL-4 levels were increased both locally in the heart and systemically, suggesting that heightened IL-4 signaling may contribute importantly to sustaining local inflammation and macrophage expansion in failing myocardium.

In both murine and human HF, the expanded cardiac CD206$^+$ macrophage population was primarily CCR2$^-$ (~80%), MHCII^{hi}, and LYVE1$^+$. In naïve[15] and in sham-operated hearts, CD206$^+$ macrophages were also primarily CCR2$^-$, albeit to much greater degrees (~95%) than in failing hearts. As LYVE1 is considered a marker of resident macrophages,[6] this suggests a predominantly resident macrophage population that is expanded in failing hearts, but also with a dual (albeit lesser) contribution from CCR2$^+$ monocyte-derived cells. Prior work has shown that after MI the absence of CCR2 expression does not exclude a monocyte origin as recruited macrophages over time may exhibit transcriptional identities nearly identical to resident

macrophages.[6] Our study design did not incorporate macrophage lineage tracing to definitively address this question. Nonetheless, our data are consistent with prior work indicating that cardiac macrophages derive from both local macrophage proliferation and recruited monocytes (locally-sourced cells comprising ~75%) in chronic ischemic HF.[3,5] Given our observations that the proportion of $CCR2^+$ cells increased significantly in failing hearts, and that cardiac macrophage abundance in post-MI HF was paralleled by similar dynamic changes in $Ly6C^{high}$ blood monocytes that source infiltrating macrophages,[3,5,6,10] we propose that the expanded and proliferative cardiac $CD206^+$macrophage population derives from both resident and recruited cells.

We evaluated the pathophysiological importance of $CD206^+$IL-4Rα^+ expansion in the failing heart by experimentally manipulating IL-4Rα signaling, which occurs largely in immune cells.[45] While both M[IL-4] and M[IL-10] macrophage polarization induced the upregulation of signature alternative macrophage activation genes, M[IL-4] polarization exclusively resulted in extraordinary upregulation of *Fizz1*, and functional myofibroblast differentiation of cMSCs, together with enhanced cMSC proliferative gene expression. Importantly, intramyocardial adoptive transfer of M[IL-4], but not M[IL-10], macrophages produced significant long-term LV chamber dilatation, dysfunction, and fibrosis in naïve recipients. Hence, IL-4-mediated activation of macrophages was sufficient to recapitulate chronic cardiac remodeling.

To establish the necessity of $CD206^+$IL-4Rα^+ macrophages in the pathogenesis of chronic LV remodeling, we evaluated the effects of myeloid IL-4Rα deletion during established HF on subsequent LV remodeling. This manipulation primarily impacted macrophages in HF, given the very low levels of IL-4Rα in neutrophils and monocytes. Notably, loss of macrophage IL-4 signaling via IL-4Rα suppressed $CD206^+$ macrophage proliferation, abrogated the progression of LV remodeling, improved LV systolic function and fibrosis, while suppressing both $CD206^+$ and $CD206^-$ macrophages in the heart as well as systemic $Ly6C^{hi}$ monocytosis in

683 the blood. Beneficial effects of macrophage IL-4Rα deletion were observed in both male and
684 female mice. Hence, $CD206^{+}IL4R\alpha^{+}$ macrophages are indispensable for sustaining a chronic
685 para-inflammatory response in failing myocardium that drives progressive cardiac remodeling in
686 HF.

687 To explore a potential therapeutic avenue, we performed *in vivo* gene silencing of IL-
688 4Rα using ASOs, an approach that primarily targeted cardiac $CD206^{+}$ macrophages given the
689 aforementioned low distribution of IL-4Rα expression observed in other myeloid and lymphoid
690 cell populations in chronic HF. IL-4Rα silencing in chronic ischemic HF very effectively depleted
691 cardiac $CD206^{+}IL\text{-}4R\alpha^{+}$ macrophages and suppressed their proliferation and phagocytic
692 capacity, while inducing impressive reverse LV remodeling with improvements in cardiac fibrosis,
693 neovascularization, and function, and suppression of both local and systemic inflammation (*e.g.*,
694 blood and cardiac $CD4^{+}$ and $CD8^{+}$ T cell levels). Taken together, our results underscore the
695 pathological effects of chronic macrophage IL-4Rα activation in the failing heart and establish
696 $CD206^{+}IL\text{-}4R\alpha^{+}$ macrophages as key mediators of pathological remodeling of the failing heart.
697 Our data support biological or pharmacological blockade of the IL-4/IL-4Rα pathway as a novel
698 immunomodulatory paradigm in HF. For instance, antagonistic antibodies against IL-4Rα are
699 currently being developed for allergic disorders in humans,[67] and could potentially be
700 repurposed for HF.

701 $CD206^{+}$ macrophage abundance in murine failing hearts (or $CD163^{+}$ macrophage
702 abundance in human HF) correlated with the extent of cardiac fibrosis in chronic HF, and a
703 prominent feature of IL-4-mediated $CD206^{+}$ macrophage activation *in vitro* and *in vivo* was the
704 induction of pro-fibrotic responses. Our data suggest that the protein FIZZ1 secreted by M[IL-4]
705 macrophages may play an important role in this crosstalk, given: 1) *in vitro* studies
706 demonstrating incredibly robust macrophage *Fizz1* upregulation upon IL-4 stimulation, 2) FIZZ1
707 dependence of the induction of cMSC myofibroblast differentiation by M[IL-4] macrophages,

potentially via DLL-4/Jagged1-Notch1 signaling, 3) exclusive expression of Fizz1 by cardiac $CD206^{+}IL\text{-}4R\alpha^{+}$ macrophages in chronic HF, and 4) exclusive expression of FIZZ3 (resistin), the human homolog of FIZZ1,[58] by $CD163^{+}IL\text{-}4R\alpha^{+}$ macrophages in human failing hearts. FIZZ1 is secreted during Th2-type immune responses in mice.[52,68] and induces myofibroblast differentiation and fibrosis in the lung,[53,54] whereas FIZZ3 induces LV fibrosis and dysfunction when overexpressed in rat heart[69] and is a serum risk prediction biomarker in HF patients.[70] Our data are consistent with a key pro-fibrotic function for FIZZ1 in the failing heart, secreted by alternatively-activated $CD206^{+}IL\text{-}4R\alpha^{+}$ macrophages as part of an overall Th2/M2-like inflammatory milieu in the failing heart.[26] The elucidation of the precise role of Fizz1/Fizz3, and the potential for therapeutic Fizz1/Fizz3 blockade in HF, will require further study.

In summary, we have established a novel immunoinflammatory framework in the failing heart with an expanded pool of alternatively activated $CD206^{+}IL\text{-}4R\alpha^{+}$ macrophages as key drivers of LV remodeling. These alternatively-activated macrophages induce a para-inflammatory, immuno-fibrotic response, in part dependent on FIZZ1 expression, that promotes cardiac fibrosis and dysfunction. Our findings identify IL-4 signaling in $CD206^{+}$ macrophages, and potentially FIZZ1/FIZZ3 elaboration, as novel and appealing therapeutic targets for immunomodulation to limit long-term cardiac remodeling in ischemic cardiomyopathy and HF.

ACKNOWLEDGEMENTS AND FUNDING

This work was supported by National Institutes of Health R01 HL157999 and HL147549 grants to SDP, and R01 HL137046 to TH.

COMPETING INTERESTS

There are no relevant author financial interests.

FIGURE LEGENDS

Figure 1. Cardiac CD206$^+$ macrophages robustly expand and express IL-4Rα in heart failure (HF). ***A***, Protocol for cardiac macrophage profiling by FACS in C57BL/6 mice at the indicated time points after non-reperfused myocardial infarction (MI) or sham operation. ***B*** and ***C***, representative flow cytometry scatter plots (***B***) and group quantitation for cardiac macrophages (F4/80$^+$MerTK$^+$), and CD206$^+$ and CD206$^-$ subpopulations (***C***) from sham and MI mice at the indicated times post-operation. Quantitation from naïve mice also shown. ***D***, Representative flow plots and group data for IL-4Rα and IL-10Rα expression in cardiac CD206$^+$ macrophages from the same mouse groups. Statistics: unpaired Student's t test; ***p*<0.01 vs respective sham group in ***C***-***D***; $^{\$\$}$*p*<0.01 vs Sham-CD206$^-$ in ***C***, $^{\$\$}$*p*<0.01 vs Sham-IL-10Rα$^+$ in ***D***. N=6-8 per group.

Figure 2. Cardiac CD206$^+$ macrophages are proliferative, primarily MHCII^{hi} and LYVE1$^+$, and correlate with LV dysfunction and fibrosis in heart failure (HF). ***A***, Representative long-axis 2-dimensional echocardiograms at end-diastole and heart trichrome stains from HF mice 8 w after non-reperfused myocardial infarction (MI) and sham controls, along with correlations between cardiac CD206$^+$ macrophage number and LV ejection fraction (LVEF), and border and remote zone (BZ and RZ) fibrosis in failing hearts. ***B***, Representative low and high magnification confocal images of failing heart (8 w post-MI) infarct, border, and remote zones (immuno)stained for CD206 (red) and collagen hybridizing peptide (CHP) (green), with quantitation of CHP-associated and -unassociated CD206$^+$ macrophages. DAPI (blue) was used to label nuclei. Scale bar 50 μm. ***C***, Flow plots and quantitation of CCR2 and LYVE1 expression in CD206$^+$ macrophages and LYVE-1 expression in CD206$^+$CCR2$^-$ macrophages in sham and HF hearts 8 w post-surgery, ***D***, Low and high magnification confocal images of CD206 (red) and Ki67 (green) immunostains of sham, and the infarct, border and remote zones of failing hearts 8 w post-surgery, and quantitation of CD206$^+$ macrophages and Ki67

758 expression frequency. Nuclei labeled by DAPI (blue); yellow arrows indicate $CD206^{+}Ki67^{+}$ cells.
759 Scale bar 50 μm. ***E***, Flow plots and quantitation of Ki67 expression in both $CD206^{+}$ and $CD206^{-}$
760 cardiac macrophages from the same groups. Statistics: Pearson R correlation test in ***Aa***;
761 unpaired Student's t test in ***C***-***E***. N=4-13 per group as indicated.

762 **Figure 3. IL-4-polarized bone marrow derived macrophages (BMDMs) induce**
763 **cardiac mesenchymal stem cell (cMSC) myofibroblast differentiation *in vitro*. *A***, Protocol
764 for BMDM polarization and cMSC treatment with macrophage conditioned medium, and
765 representative flow plots of F4/80 and CD206 expression in polarized BMDMs. ***B***, Expression of
766 the indicated genes in M0, M[IL-4], and M[IL-10] macrophages 24 h after polarization. ***C***,
767 Expression of the indicated genes in cMSCs treated with M0, M[IL-4], and M[IL-10] conditioned
768 media for the indicated times, and representative cMSC-imbued collagen gel contraction assays
769 upon exposure to M0, M[IL-4], and M[IL-10] conditioned media, or media alone (Ctrl), and
770 quantitation of gel areas. Statistics: 1-way ANOVA with post-hoc Tukey's multiple comparison
771 test; * $p<0.05$, ** $p<0.01$ vs. M0. N=5-6/group.

772 **Figure 4. Adoptive transfer of M[IL-4] macrophages to naïve hearts induces**
773 **cardiac dysfunction and fibrosis. *A***, Protocol for intramyocardial adoptive transfer of M0,
774 M[IL-4], and M[IL-10] bone marrow derived macrophages (BMDMs) or PBS vehicle to naïve
775 mice. ***B***, M-mode echocardiograms of M0, M[IL-4], and M[IL-10] BMDM recipient mice 4 w post-
776 transfer (PBS control), along with group data for LV end-systolic and end-diastolic volume (ESV
777 and EDV), ejection fraction (EF) at indicated times post-transfer, and for echocardiographic LV
778 mass normalized to tibia length (TL), and end-diastolic interventricular septal and posterior wall
779 thickness (IVSWT and PWT) at 4 w post-transfer. ***C***, Representative trichrome stains of
780 recipient hearts at 4 w post-transfer and corresponding quantitation of cardiac fibrosis. ***D***, *Top*,
781 cardiac wheat-germ agglutinin (WGA, red) staining and quantitation of myocyte cross-sectional
782 area; *Middle*, low and high magnification images of TUNEL (green) stained nuclei in
783 cardiomyocytes (α-Actinin, Red) and quantitation of apoptotic myocyte nuclei; and *Bottom*, Low

and high magnification confocal images of CD206 (red) and CD45.2 (gray) immunostains and quantitation of $CD206^{+}CD45.2^{+}$ and $CD206^{+}CD45.2^{-}$ macrophages in recipient hearts, all at 4 w post-transfer. Green arrows indicate apoptotic myocyte nuclei, red arrows indicate $CD206^{+}CD45.2^{-}$ cells, and white arrows indicate $CD206^{+}CD45.2^{+}$ cells. DAPI (blue) was used to label nuclei. ***E***, Low and high magnification confocal images of CD206 (red) and CD45.2 (gray) immunostaining and CHP staining (green), and quantitation of CHP-associated and -unassociated, $CD45.2^{+}$ and $CD45.2^{-}$ $CD206^{+}$ macrophage ratios in M[IL-4] recipient hearts 4 w post-transfer. Nuclei were labeled by DAPI (blue). Red arrows indicate CHP-unassociated $CD206^{+}CD45.2^{-}$ cells and white arrows indicate CHP-unassociated $CD206^{+}CD45.2^{+}$ cells. Statistics: repeated-measures 1-way ANOVA with post-hoc Dunnett's multiple comparison test for time series within groups in ***B***, 1-way ANOVA with post-hoc Tukey's multiple comparison test between groups in ***B-D***, and unpaired Student's t test in ***E***; *p<0.05, **p<0.01 M[IL-4] vs. PBS; $^{\#}p$<0.05, $^{\#\#}p$<0.01 M[IL-4] vs. M0; $^{\$}p$<0.05, $^{\$\$}p$<0.01 M[IL-4] vs. M[IL-10]; $^{\Delta}p$<0.05, $^{\Delta\Delta}p$<0.01 vs. Bsln. N=6-8 per group as indicated.

Figure 5. Myeloid-specific IL-4Rα deletion suppresses cardiac $CD206^{+}$ macrophages and alleviates LV remodeling in heart failure (HF). ***A***, Protocol for myeloid-specific IL-4Rα ablation in IL-4R$\alpha^{f/f}$LysM-Cre^{ERT2} sham and HF mice (IL-4R$\alpha^{f/f}$ mouse control) with tamoxifen administration in diet from 4 to 10 w post-MI or sham surgery. ***B***, Representative long-axis 2D echocardiograms at end-diastole from male sham and HF mice after 6 w of tamoxifen (10 w post-surgery), along with directional changes in LV end-diastolic and end-systolic volume (EDV and ESV) and LV ejection fraction (EF) over this time. ***C***, Representative trichrome stains of hearts from IL-4R$\alpha^{f/f}$ and IL-4R$\alpha^{f/f}$LysM-Cre^{ERT2} sham and HF mice after 6 w of tamoxifen (10 w post-surgery) along with fibrosis quantitation in the border and remote zone (BZ and RZ). ***D*** and ***E*****,** Representative flow plots for cardiac macrophages ($F4/80^{+}MerTK^{+}$), $CD206^{+}$ macrophages, and IL-4Rα and IL-10Rα expressing $CD206^{+}$ subpopulations in IL-4R$\alpha^{f/f}$

and IL-4Rα$^{f/f}$LysM-Cre^{ERT2} HF mice, along with quantitative group data from both sham and HF male mice after 6 w of tamoxifen. ***F***, Representative flow plots and quantitation of Ki67 expression in cardiac CD206^{+} and CD206^{-} macrophages from IL-4Rα$^{f/f}$ and IL-4Rα$^{f/f}$LysM-Cre^{ERT2} HF mice given tamoxifen for 6 w. Statistics: 2-way ANOVA with post-hoc Tukey's multiple comparisons between groups in ***B-E***; unpaired Student's t test in in ***F***. N=7-11 per group.

Figure 6. *In vivo* IL-4Rα silencing depletes cardiac CD206^{+} macrophages and reverses LV remodeling in heart failure (HF). ***A***, Protocol for treatment with IL-4Rα antisense oligonucleotides (ASOs) or mismatched (MM) control oligonucleotides (oligo) in HF mice from 4 to 8 w after non-reperfused myocardial infarction (MI) (sham controls). ***B***, Representative long-axis 2-dimensional echocardiograms at end-diastole from sham and HF mice treated with IL-4Rα ASOs or MM Oligos for 4 w (8 w post-surgery timepoint). Also shown are group data for LV end-diastolic and end-systolic volume (EDV and ESV) and ejection fraction (EF) over the treatment period. ***C***, Gross images of hearts from IL-4Rα ASO- and MM Oligo-treated sham and HF mice, and group data for lung and heart weight (LW and HW) normalized to tibia length (TL). ***D*****,** Representative trichrome stains of IL-4Rα ASO- and MM Oligo-treated sham and failing hearts, and fibrosis quantitation in the border and remote zone (BZ and RZ). ***E***, Representative cardiac isolectin B4 (IB4, green) and WGA (red) staining and quantitation of myocyte cross-sectional area and capillary:myocyte ratio in the LV RZ from IL-4Rα ASO- and MM Oligo-treated sham and HF mice. ***F***, *Left*, quantitation of cardiac CD206^{+} macrophages, and *Middle* and *Right*, flow plots and quantitation of IL-4Rα and IL-10Rα expressing subpopulations, in sham and HF mice treated with IL-4Rα ASOs or MM Oligos for 4 w. ***G***, Serum levels of IL-4 and IL-10 from the same groups. ***H*** and ***I***, Representative flow cytometry histograms, dot plots, and quantitation of cardiac Ki67^{+} (***H***) or bioparticle^{+} (***I***) CD206^{+} and CD206^{-} macrophages in IL-4Rα ASO- and MM Oligo- treated HF mice. Statistics: repeated-measures 1-way ANOVA with post-hoc Dunnett's

multiple comparison test for time series within groups in ***B***; 2-way ANOVA with post-hoc Tukey's multiple comparisons between groups in ***B-F, H, I***; unpaired Student's t test in ***G***. ***p*<0.01 vs. respective Sham-MM Oligo; $^{\#\#}p$<0.01 vs. HF-MM Oligo at the same week post-surgery; $^{\Delta}p$<0.05, $^{\Delta\Delta}p$<0.01 vs. respective 4 w timepoint. N=5-8 per group.

Figure 7. Fizz1 is essential for CD206^{+} macrophage-induced myofibroblast differentiation of cardiac mesenchymal stem cells (cMSCs). ***A***, cMSC-imbued collagen gel contraction assays upon exposure to M[IL-4] bone marrow-derived macrophage (BMDM) conditioned media or media alone control (Ctrl) containing isotype IgG or anti-Fizz1 antibody with corresponding quantitation of gel areas. ***B***, cMSC gel contraction assays upon exposure to wild-type (WT) and Fizz1$^{-/-}$ M0 or M[IL-4] BMDM conditioned media, and quantitation of gel areas. N=3-5 per group for ***A-B***. ***C***, cMSC DLL-4 and Jagged1 gene expression after 30 minutes of treatment with either vehicle (Ctrl) or recombinant mouse (rm) Fizz1 50 ng/ml and 100 ng/ml. ***D***, Immunoblotting and group quantitation for Notch1, Notch intracellular domain (NICD), and α-smooth muscle actin (α-SMA) protein expression in cMSCs treated with either vehicle Ctrl or rmFizz1 for 24 h following scrambled or Notch1 siRNA transfection. GAPDH loading control. ***E***, Representative low and high magnification confocal images of immunostains for CD206 (red), IL-4Rα (white) and Fizz1 (green) of hearts from sham and HF hearts (border zone) from MM Oligo- or IL-4Rα ASO-treated mice, with quantitation of CD206^{+}IL-4Rα^{+}Fizz1^{+} and CD206^{+}IL-4Rα^{-}Fizz1^{-} macrophages, and IL-4Rα fluorescent intensity (arbitrary units [a.u.]) n=5-8/group. DAPI (blue) was used to label nuclei. Red arrows indicate CD206^{+}IL-4Rα^{-}Fizz1^{-} cells and yellow arrows indicate CD206^{+}IL-4Rα^{+}Fizz1^{+} cells. Statistics: 2-way ANOVA followed by Tukey's multiple comparison test, except 1-way ANOVA followed by Tukey's multiple comparison test in panel ***C***; **p*<0.05, ***p*<0.01 vs. Ctrl in ***C***; ***p*<0.01 vs. Ctrl-scramble siRNA, $^{\#\#}p$<0.01 vs. rmFIZZ1-scramble siRNA in ***D*.** N=6 per group. MM, mismatched; ASO, antisense oligonucleotide.

Figure 8. Alternatively activated cardiac macrophages expand, express IL-4Rα and FIZZ3, and directly correlate with fibrosis in human heart failure (HF). ***A***, Representative flow plots for $CD45^+$Autofluorescence(Auto)$^+CD64^+CD206^+$ macrophages and their CCR2 expression, and group quantitation for $CD206^+$ macrophages in normal control (Ctrl; n=3) and failing (n=13) human hearts (from LV assist device core tissue). ***B***, Representative trichrome stains (*Top*) and low and high magnification (immuno)stains for CD163 (red) and collagen-hybridizing peptide (CHP, green) (*Bottom*) of Ctrl and failing human hearts, with corresponding quantitation of cardiac fibrosis (10 Ctrl, 19 failing hearts) and CHP-associated and -unassociated $CD163^+$ macrophage frequency (n=7/group). ***C***, Low and high magnification confocal images of immunostains for CD163 (white), IL-4Rα (red) and Fizz3 (green) in normal (Ctrl; n=4) and failing (n=8) human hearts (HF), and quantitation of IL-$4R\alpha^+Fizz3^+$ and IL-$4R\alpha^-Fizz3^-$ $CD163^+$ macrophages. DAPI (blue) was used to label nuclei. White arrows indicate $CD163^+$IL-$4R\alpha^-Fizz3^-$ cells, and yellow arrows indicate $CD163^+$IL-$4R\alpha^+Fizz3^+$ cells. Also shown is the correlation between $CD163^+$ macrophage abundance and LV fibrosis in human HF, n=19. Statistics: Mann-Whitney test in ***A***; unpaired Student's t test in ***B-C;*** Pearson R correlation test in ***C, lower right panel***.

REFERENCES

1. Adamo L, Rocha-Resende C, Prabhu SD, Mann DL. Reappraising the role of inflammation in heart failure. *Nat Rev Cardiol*. 2020;17:269-285. doi: 10.1038/s41569-019-0315-x
2. Bajpai G, Schneider C, Wong N, Bredemeyer A, Hulsmans M, Nahrendorf M, Epelman S, Kreisel D, Liu Y, Itoh A, et al. The human heart contains distinct macrophage subsets with divergent origins and functions. *Nat Med*. 2018;24:1234-1245. doi: 10.1038/s41591-018-0059-x
3. Heidt T, Courties G, Dutta P, Sager HB, Sebas M, Iwamoto Y, Sun Y, Da Silva N, Panizzi P, van der Laan AM, et al. Differential contribution of monocytes to heart macrophages in steady-state and after myocardial infarction. *Circ Res*. 2014;115:284-295. doi: 10.1161/CIRCRESAHA.115.303567
4. Ismahil MA, Hamid T, Bansal SS, Patel B, Kingery JR, Prabhu SD. Remodeling of the mononuclear phagocyte network underlies chronic inflammation and disease progression in heart failure: critical importance of the cardiosplenic axis. *Circ Res*. 2014;114:266-282. doi: 10.1161/CIRCRESAHA.113.301720
5. Sager HB, Hulsmans M, Lavine KJ, Moreira MB, Heidt T, Courties G, Sun Y, Iwamoto Y, Tricot B, Khan OF, et al. Proliferation and Recruitment Contribute to Myocardial Macrophage Expansion in Chronic Heart Failure. *Circ Res*. 2016;119:853-864. doi: 10.1161/CIRCRESAHA.116.309001
6. Dick SA, Macklin JA, Nejat S, Momen A, Clemente-Casares X, Althagafi MG, Chen J, Kantores C, Hosseinzadeh S, Aronoff L, et al. Self-renewing resident cardiac macrophages limit adverse remodeling following myocardial infarction. *Nat Immunol*. 2019;20:29-39. doi: 10.1038/s41590-018-0272-2
7. Epelman S, Lavine KJ, Beaudin AE, Sojka DK, Carrero JA, Calderon B, Brija T, Gautier EL, Ivanov S, Satpathy AT, et al. Embryonic and adult-derived resident cardiac macrophages are maintained through distinct mechanisms at steady state and during inflammation. *Immunity*. 2014;40:91-104. doi: 10.1016/j.immuni.2013.11.019
8. Lavine KJ, Epelman S, Uchida K, Weber KJ, Nichols CG, Schilling JD, Ornitz DM, Randolph GJ, Mann DL. Distinct macrophage lineages contribute to disparate patterns of cardiac recovery and remodeling in the neonatal and adult heart. *Proc Natl Acad Sci U S A*. 2014;111:16029-16034. doi: 10.1073/pnas.1406508111
9. Bajpai G, Bredemeyer A, Li W, Zaitsev K, Koenig AL, Lokshina I, Mohan J, Ivey B, Hsiao HM, Weinheimer C, et al. Tissue Resident CCR2- and CCR2+ Cardiac Macrophages Differentially Orchestrate Monocyte Recruitment and Fate Specification Following Myocardial Injury. *Circ Res*. 2019;124:263-278. doi: 10.1161/CIRCRESAHA.118.314028
10. Hilgendorf I, Gerhardt LM, Tan TC, Winter C, Holderried TA, Chousterman BG, Iwamoto Y, Liao R, Zirlik A, Scherer-Crosbie M, et al. Ly-6Chigh monocytes depend on Nr4a1 to balance both inflammatory and reparative phases in the infarcted myocardium. *Circ Res*. 2014;114:1611-1622. doi: 10.1161/CIRCRESAHA.114.303204
11. Prabhu SD, Frangogiannis NG. The Biological Basis for Cardiac Repair After Myocardial Infarction: From Inflammation to Fibrosis. *Circ Res*. 2016;119:91-112. doi: 10.1161/CIRCRESAHA.116.303577
12. Prabhu SD. The Cardiosplenic Axis Is Essential for the Pathogenesis of Ischemic Heart Failure. *Trans Am Clin Climatol Assoc*. 2018;129:202-214.
13. Revelo XS, Parthiban P, Chen C, Barrow F, Fredrickson G, Wang H, Yucel D, Herman A, van Berlo JH. Cardiac Resident Macrophages Prevent Fibrosis and Stimulate Angiogenesis. *Circ Res*. 2021;129:1086-1101. doi: 10.1161/CIRCRESAHA.121.319737
14. Martini E, Kunderfranco P, Peano C, Carullo P, Cremonesi M, Schorn T, Carriero R, Termanini A, Colombo FS, Jachetti E, et al. Single-Cell Sequencing of Mouse Heart

Immune Infiltrate in Pressure Overload-Driven Heart Failure Reveals Extent of Immune Activation. *Circulation*. 2019;140:2089-2107. doi: 10.1161/CIRCULATIONAHA.119.041694

15. Shiraishi M, Shintani Y, Shintani Y, Ishida H, Saba R, Yamaguchi A, Adachi H, Yashiro K, Suzuki K. Alternatively activated macrophages determine repair of the infarcted adult murine heart. *J Clin Invest*. 2016;126:2151-2166. doi: 10.1172/JCI85782
16. Yan X, Anzai A, Katsumata Y, Matsuhashi T, Ito K, Endo J, Yamamoto T, Takeshima A, Shinmura K, Shen W, et al. Temporal dynamics of cardiac immune cell accumulation following acute myocardial infarction. *J Mol Cell Cardiol*. 2013;62:24-35. doi: 10.1016/j.yjmcc.2013.04.023
17. Leblond AL, Klinkert K, Martin K, Turner EC, Kumar AH, Browne T, Caplice NM. Systemic and Cardiac Depletion of M2 Macrophage through CSF-1R Signaling Inhibition Alters Cardiac Function Post Myocardial Infarction. *PLoS One*. 2015;10:e0137515. doi: 10.1371/journal.pone.0137515
18. Gordon S, Martinez FO. Alternative activation of macrophages: mechanism and functions. *Immunity*. 2010;32:593-604. doi: 10.1016/j.immuni.2010.05.007
19. Martinez FO, Gordon S. The M1 and M2 paradigm of macrophage activation: time for reassessment. *F1000Prime Rep*. 2014;6:13. doi: 10.12703/P6-13
20. Murray PJ, Allen JE, Biswas SK, Fisher EA, Gilroy DW, Goerdt S, Gordon S, Hamilton JA, Ivashkiv LB, Lawrence T, et al. Macrophage activation and polarization: nomenclature and experimental guidelines. *Immunity*. 2014;41:14-20. doi: 10.1016/j.immuni.2014.06.008
21. Wynn TA, Vannella KM. Macrophages in Tissue Repair, Regeneration, and Fibrosis. *Immunity*. 2016;44:450-462. doi: 10.1016/j.immuni.2016.02.015
22. Tugal D, Liao X, Jain MK. Transcriptional control of macrophage polarization. *Arterioscler Thromb Vasc Biol*. 2013;33:1135-1144. doi: 10.1161/ATVBAHA.113.301453
23. Mantovani A, Sica A, Sozzani S, Allavena P, Vecchi A, Locati M. The chemokine system in diverse forms of macrophage activation and polarization. *Trends Immunol*. 2004;25:677-686. doi: 10.1016/j.it.2004.09.015
24. Shintani Y, Ito T, Fields L, Shiraishi M, Ichihara Y, Sato N, Podaru M, Kainuma S, Tanaka H, Suzuki K. IL-4 as a Repurposed Biological Drug for Myocardial Infarction through Augmentation of Reparative Cardiac Macrophages: Proof-of-Concept Data in Mice. *Sci Rep*. 2017;7:6877. doi: 10.1038/s41598-017-07328-z
25. Tang PM, Nikolic-Paterson DJ, Lan HY. Macrophages: versatile players in renal inflammation and fibrosis. *Nat Rev Nephrol*. 2019;15:144-158. doi: 10.1038/s41581-019-0110-2
26. Bansal SS, Ismahil MA, Goel M, Patel B, Hamid T, Rokosh G, Prabhu SD. Activated T Lymphocytes are Essential Drivers of Pathological Remodeling in Ischemic Heart Failure. *Circ Heart Fail*. 2017;10:e003688. doi: 10.1161/CIRCHEARTFAILURE.116.003688
27. Herbert DR, Holscher C, Mohrs M, Arendse B, Schwegmann A, Radwanska M, Leeto M, Kirsch R, Hall P, Mossmann H, et al. Alternative macrophage activation is essential for survival during schistosomiasis and downmodulates T helper 1 responses and immunopathology. *Immunity*. 2004;20:623-635. doi: 10.1016/s1074-7613(04)00107-4
28. Vishlaghi N, Guo L, Griswold-Wheeler D, Sun Y, Booker C, Crossley JL, Bancroft AC, Juan C, Korlakunta S, Ramesh S, et al. Vegfc-expressing cells form heterotopic bone after musculoskeletal injury. *Cell Rep*. 2024;43:114049. doi: 10.1016/j.celrep.2024.114049
29. Bansal SS, Ismahil MA, Goel M, Zhou G, Rokosh G, Hamid T, Prabhu SD. Dysfunctional and Proinflammatory Regulatory T-Lymphocytes Are Essential for Adverse Cardiac Remodeling in Ischemic Cardiomyopathy. *Circulation*. 2019;139:206-221. doi: 10.1161/CIRCULATIONAHA.118.036065

30. Hamid T, Gu Y, Ortines RV, Bhattacharya C, Wang G, Xuan YT, Prabhu SD. Divergent tumor necrosis factor receptor-related remodeling responses in heart failure: role of nuclear factor-kappaB and inflammatory activation. *Circulation*. 2009;119:1386-1397. doi: 10.1161/CIRCULATIONAHA.108.802918
31. Wang G, Hamid T, Keith RJ, Zhou G, Partridge CR, Xiang X, Kingery JR, Lewis RK, Li Q, Rokosh DG, et al. Cardioprotective and antiapoptotic effects of heme oxygenase-1 in the failing heart. *Circulation*. 2010;121:1912-1925. doi: 10.1161/CIRCULATIONAHA.109.905471
32. Patel B, Bansal SS, Ismahil MA, Hamid T, Rokosh G, Mack M, Prabhu SD. CCR2(+) Monocyte-Derived Infiltrating Macrophages Are Required for Adverse Cardiac Remodeling During Pressure Overload. *JACC Basic Transl Sci*. 2018;3:230-244. doi: 10.1016/j.jacbts.2017.12.006
33. Hamid T, Xu Y, Ismahil MA, Rokosh G, Jinno M, Zhou G, Wang Q, Prabhu SD. Cardiac Mesenchymal Stem Cells Promote Fibrosis and Remodeling in Heart Failure: Role of PDGF Signaling. *JACC Basic Transl Sci*. 2022;7:465-483. doi: 10.1016/j.jacbts.2022.01.004
34. Wang Q, Wang S, Sun Z. Kidney-Specific Klotho Gene Deletion Causes Aortic Aneurysm via Hyperphosphatemia. *Hypertension*. 2021;78:308-319. doi: 10.1161/HYPERTENSIONAHA.121.17299
35. Tang L, Zhang H, Wang C, Li H, Zhang Q, Bai J. M2A and M2C Macrophage Subsets Ameliorate Inflammation and Fibroproliferation in Acute Lung Injury Through Interleukin 10 Pathway. *Shock*. 2017;48:119-129. doi: 10.1097/SHK.0000000000000820
36. Hamid T, Xu Y, Ismahil MA, Li Q, Jones SP, Bhatnagar A, Bolli R, Prabhu SD. TNF receptor signaling inhibits cardiomyogenic differentiation of cardiac stem cells and promotes a neuroadrenergic-like fate. *Am J Physiol Heart Circ Physiol*. 2016;311:H1189-H1201. doi: 10.1152/ajpheart.00904.2015
37. Bujak M, Ratkaj I, Markova-Car E, Jurisic D, Horvatic A, Vucinic S, Lerga J, Baus-Loncar M, Pavelic K, Kraljevic Pavelic S. Inflammatory Gene Expression Upon TGF-beta1-Induced p38 Activation in Primary Dupuytren's Disease Fibroblasts. *Front Mol Biosci*. 2015;2:68. doi: 10.3389/fmolb.2015.00068
38. Covarrubias R, Ismahil MA, Rokosh G, Hamid T, Accornero F, Singh H, Gumina RJ, Prabhu SD, Bansal SS. Optimized protocols for isolation, fixation, and flow cytometric characterization of leukocytes in ischemic hearts. *Am J Physiol Heart Circ Physiol*. 2019;317:H658-H666. doi: 10.1152/ajpheart.00137.2019
39. Trouplin V, Boucherit N, Gorvel L, Conti F, Mottola G, Ghigo E. Bone marrow-derived macrophage production. *J Vis Exp*. 2013:e50966. doi: 10.3791/50966
40. Ripple MJ, You D, Honnegowda S, Giaimo JD, Sewell AB, Becnel DM, Cormier SA. Immunomodulation with IL-4R alpha antisense oligonucleotide prevents respiratory syncytial virus-mediated pulmonary disease. *J Immunol*. 2010;185:4804-4811. doi: 10.4049/jimmunol.1000484
41. Weng SY, Wang X, Vijayan S, Tang Y, Kim YO, Padberg K, Regen T, Molokanova O, Chen T, Bopp T, et al. IL-4 Receptor Alpha Signaling through Macrophages Differentially Regulates Liver Fibrosis Progression and Reversal. *EBioMedicine*. 2018;29:92-103. doi: 10.1016/j.ebiom.2018.01.028
42. Nahrendorf M, Swirski FK, Aikawa E, Stangenberg L, Wurdinger T, Figueiredo JL, Libby P, Weissleder R, Pittet MJ. The healing myocardium sequentially mobilizes two monocyte subsets with divergent and complementary functions. *J Exp Med*. 2007;204:3037-3047. doi: 10.1084/jem.20070885
43. Bakhshian Nik A, Alvarez-Argote S, O'Meara CC. Interleukin 4/13 signaling in cardiac regeneration and repair. *Am J Physiol Heart Circ Physiol*. 2022;323:H833-H844. doi: 10.1152/ajpheart.00310.2022

44. Shankar A, McAlees JW, Lewkowich IP. Modulation of IL-4/IL-13 cytokine signaling in the context of allergic disease. *J Allergy Clin Immunol*. 2022;150:266-276. doi: 10.1016/j.jaci.2022.06.012
45. Junttila IS. Tuning the Cytokine Responses: An Update on Interleukin (IL)-4 and IL-13 Receptor Complexes. *Front Immunol*. 2018;9:888. doi: 10.3389/fimmu.2018.00888
46. Krawiec P, Pawlowska-Kamieniak A, Pac-Kozuchowska E. Interleukin 10 and interleukin 10 receptor in paediatric inflammatory bowel disease: from bench to bedside lesson. *J Inflamm (Lond)*. 2021;18:13. doi: 10.1186/s12950-021-00279-3
47. Walter MR. The molecular basis of IL-10 function: from receptor structure to the onset of signaling. *Curr Top Microbiol Immunol*. 2014;380:191-212. doi: 10.1007/978-3-662-43492-5_9
48. Jones B, Debski A, Hans CP, Go MR, Agarwal G. Structurally abnormal collagen fibrils in abdominal aortic aneurysm resist platelet adhesion. *J Thromb Haemost*. 2022;20:470-477. doi: 10.1111/jth.15576
49. Cao Q, Wang Y, Zheng D, Sun Y, Wang Y, Lee VW, Zheng G, Tan TK, Ince J, Alexander SI, et al. IL-10/TGF-beta-modified macrophages induce regulatory T cells and protect against adriamycin nephrosis. *J Am Soc Nephrol*. 2010;21:933-942. doi: 10.1681/ASN.2009060592
50. Roszer T. Understanding the Mysterious M2 Macrophage through Activation Markers and Effector Mechanisms. *Mediators Inflamm*. 2015;2015:816460. doi: 10.1155/2015/816460
51. Nair MG, Du Y, Perrigoue JG, Zaph C, Taylor JJ, Goldschmidt M, Swain GP, Yancopoulos GD, Valenzuela DM, Murphy A, et al. Alternatively activated macrophage-derived RELM-{alpha} is a negative regulator of type 2 inflammation in the lung. *J Exp Med*. 2009;206:937-952. doi: 10.1084/jem.20082048
52. Nair MG, Gallagher IJ, Taylor MD, Loke P, Coulson PS, Wilson RA, Maizels RM, Allen JE. Chitinase and Fizz family members are a generalized feature of nematode infection with selective upregulation of Ym1 and Fizz1 by antigen-presenting cells. *Infect Immun*. 2005;73:385-394. doi: 10.1128/IAI.73.1.385-394.2005
53. Liu T, Hu B, Choi YY, Chung M, Ullenbruch M, Yu H, Lowe JB, Phan SH. Notch1 signaling in FIZZ1 induction of myofibroblast differentiation. *Am J Pathol*. 2009;174:1745-1755. doi: 10.2353/ajpath.2009.080618
54. Liu T, Yu H, Ullenbruch M, Jin H, Ito T, Wu Z, Liu J, Phan SH. The in vivo fibrotic role of FIZZ1 in pulmonary fibrosis. *PLoS One*. 2014;9:e88362. doi: 10.1371/journal.pone.0088362
55. Jenkins SJ, Ruckerl D, Thomas GD, Hewitson JP, Duncan S, Brombacher F, Maizels RM, Hume DA, Allen JE. IL-4 directly signals tissue-resident macrophages to proliferate beyond homeostatic levels controlled by CSF-1. *J Exp Med*. 2013;210:2477-2491. doi: 10.1084/jem.20121999
56. Rizzo P, Miele L, Ferrari R. The Notch pathway: a crossroad between the life and death of the endothelium. *Eur Heart J*. 2013;34:2504-2509. doi: 10.1093/eurheartj/ehs141
57. Talele NP, Fradette J, Davies JE, Kapus A, Hinz B. Expression of alpha-Smooth Muscle Actin Determines the Fate of Mesenchymal Stromal Cells. *Stem Cell Reports*. 2015;4:1016-1030. doi: 10.1016/j.stemcr.2015.05.004
58. Lurier EB, Dalton D, Dampier W, Raman P, Nassiri S, Ferraro NM, Rajagopalan R, Sarmady M, Spiller KL. Transcriptome analysis of IL-10-stimulated (M2c) macrophages by next-generation sequencing. *Immunobiology*. 2017;222:847-856. doi: 10.1016/j.imbio.2017.02.006
59. Pine GM, Batugedara HM, Nair MG. Here, there and everywhere: Resistin-like molecules in infection, inflammation, and metabolic disorders. *Cytokine*. 2018;110:442-451. doi: 10.1016/j.cyto.2018.05.014

60. Etzerodt A, Moestrup SK. CD163 and inflammation: biological, diagnostic, and therapeutic aspects. *Antioxid Redox Signal*. 2013;18:2352-2363. doi: 10.1089/ars.2012.4834
61. Frangogiannis NG. Cardiac fibrosis. *Cardiovasc Res*. 2021;117:1450-1488. doi: 10.1093/cvr/cvaa324
62. Pechkovsky DV, Prasse A, Kollert F, Engel KM, Dentler J, Luttmann W, Friedrich K, Muller-Quernheim J, Zissel G. Alternatively activated alveolar macrophages in pulmonary fibrosis-mediator production and intracellular signal transduction. *Clin Immunol*. 2010;137:89-101. doi: 10.1016/j.clim.2010.06.017
63. Wang J, Xu L, Xiang Z, Ren Y, Zheng X, Zhao Q, Zhou Q, Zhou Y, Xu L, Wang Y. Microcystin-LR ameliorates pulmonary fibrosis via modulating CD206(+) M2-like macrophage polarization. *Cell Death Dis*. 2020;11:136. doi: 10.1038/s41419-020-2329-z
64. Carlson S, Helterline D, Asbe L, Dupras S, Minami E, Farris S, Stempien-Otero A. Cardiac macrophages adopt profibrotic/M2 phenotype in infarcted hearts: Role of urokinase plasminogen activator. *J Mol Cell Cardiol*. 2017;108:42-49. doi: 10.1016/j.yjmcc.2016.05.016
65. Sieweke MH, Allen JE. Beyond stem cells: self-renewal of differentiated macrophages. *Science*. 2013;342:1242974. doi: 10.1126/science.1242974
66. Martinez FO, Helming L, Milde R, Varin A, Melgert BN, Draijer C, Thomas B, Fabbri M, Crawshaw A, Ho LP, et al. Genetic programs expressed in resting and IL-4 alternatively activated mouse and human macrophages: similarities and differences. *Blood*. 2013;121:e57-69. doi: 10.1182/blood-2012-06-436212
67. Kim JE, Jung K, Kim JA, Kim SH, Park HS, Kim YS. Engineering of anti-human interleukin-4 receptor alpha antibodies with potent antagonistic activity. *Sci Rep*. 2019;9:7772. doi: 10.1038/s41598-019-44253-9
68. Holcomb IN, Kabakoff RC, Chan B, Baker TW, Gurney A, Henzel W, Nelson C, Lowman HB, Wright BD, Skelton NJ, et al. FIZZ1, a novel cysteine-rich secreted protein associated with pulmonary inflammation, defines a new gene family. *EMBO J*. 2000;19:4046-4055. doi: 10.1093/emboj/19.15.4046
69. Chemaly ER, Hadri L, Zhang S, Kim M, Kohlbrenner E, Sheng J, Liang L, Chen J, P KR, Hajjar RJ, et al. Long-term in vivo resistin overexpression induces myocardial dysfunction and remodeling in rats. *J Mol Cell Cardiol*. 2011;51:144-155. doi: 10.1016/j.yjmcc.2011.04.006
70. Takeishi Y, Niizeki T, Arimoto T, Nozaki N, Hirono O, Nitobe J, Watanabe T, Takabatake N, Kubota I. Serum resistin is associated with high risk in patients with congestive heart failure--a novel link between metabolic signals and heart failure. *Circ J*. 2007;71:460-464. doi: 10.1253/circj.71.460

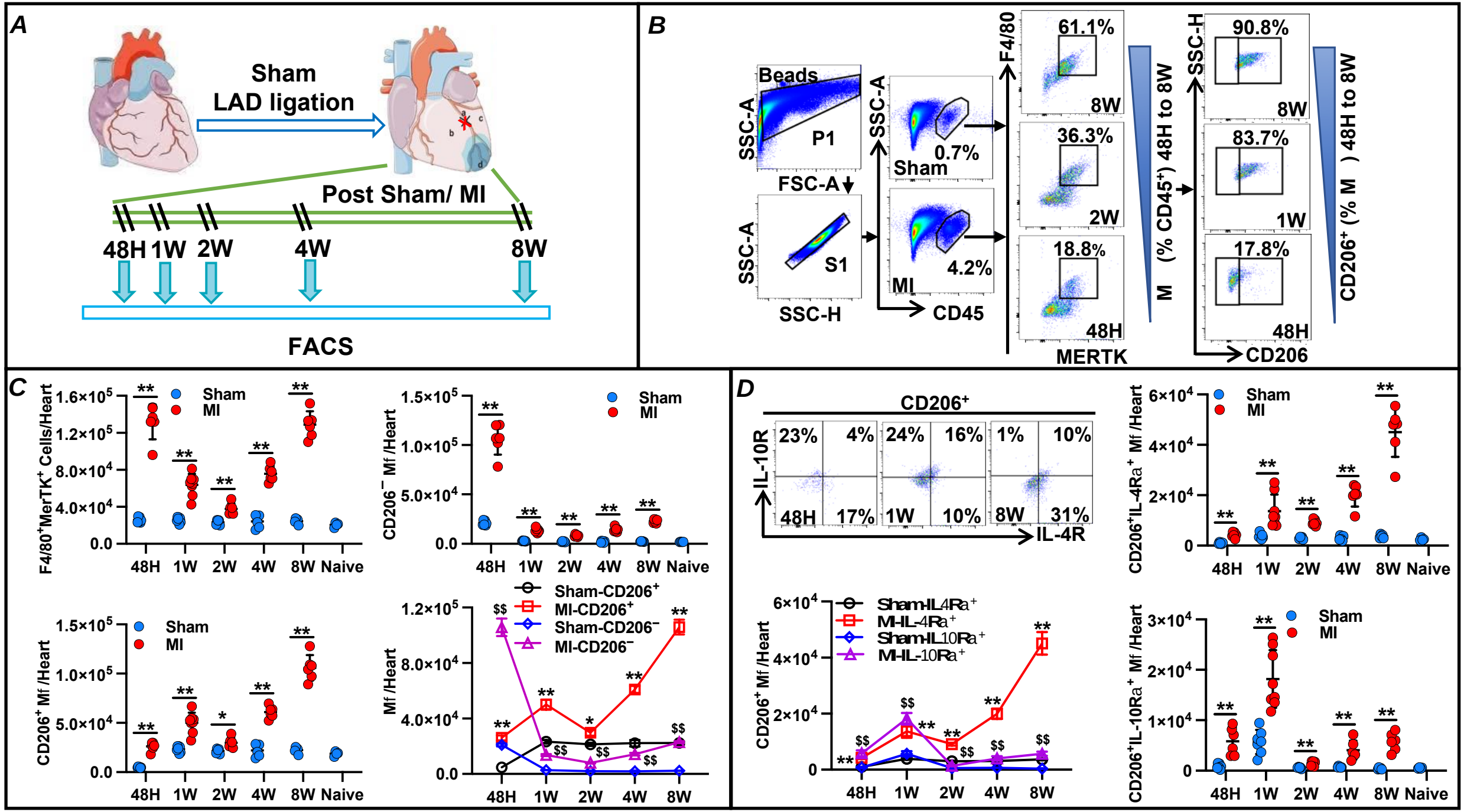
A
Sham
LAD ligation
Post Sham/ MI
48H 1W 2W 4W 8W
FACS
B
Beads
SSC-A
P1
FSC-A
SSC-A
S1
SSC-H
SSC-A
Sham
0.7%
MI
4.2%
CD45
F4/80
61.1%
8W
36.3%
2W
18.8%
48H
MERTK
M (% CD45+) 48H to 8W
SSC-H
90.8%
8W
83.7%
1W
17.8%
48H
CD206
CD206+ (% M) 48H to 8W
C
F4/80+MerTK+ Cells/Heart
Sham
MI
48H 1W 2W 4W 8W Naive
CD206− Mf /Heart
CD206+ Mf /Heart
Mf /Heart
Sham-CD206+
MI-CD206+
Sham-CD206−
MI-CD206−
D
CD206+
IL-10R
IL-4R
23%
4%
24%
16%
1%
10%
48H
17%
1W
10%
8W
31%
CD206+IL-4Ra+ Mf /Heart
CD206+ Mf /Heart
Sham-IL4Ra+
MI-IL-4Ra+
Sham-IL10Ra+
MI-IL-10Ra+
CD206+IL-10Ra+ Mf /Heart

Figure 1

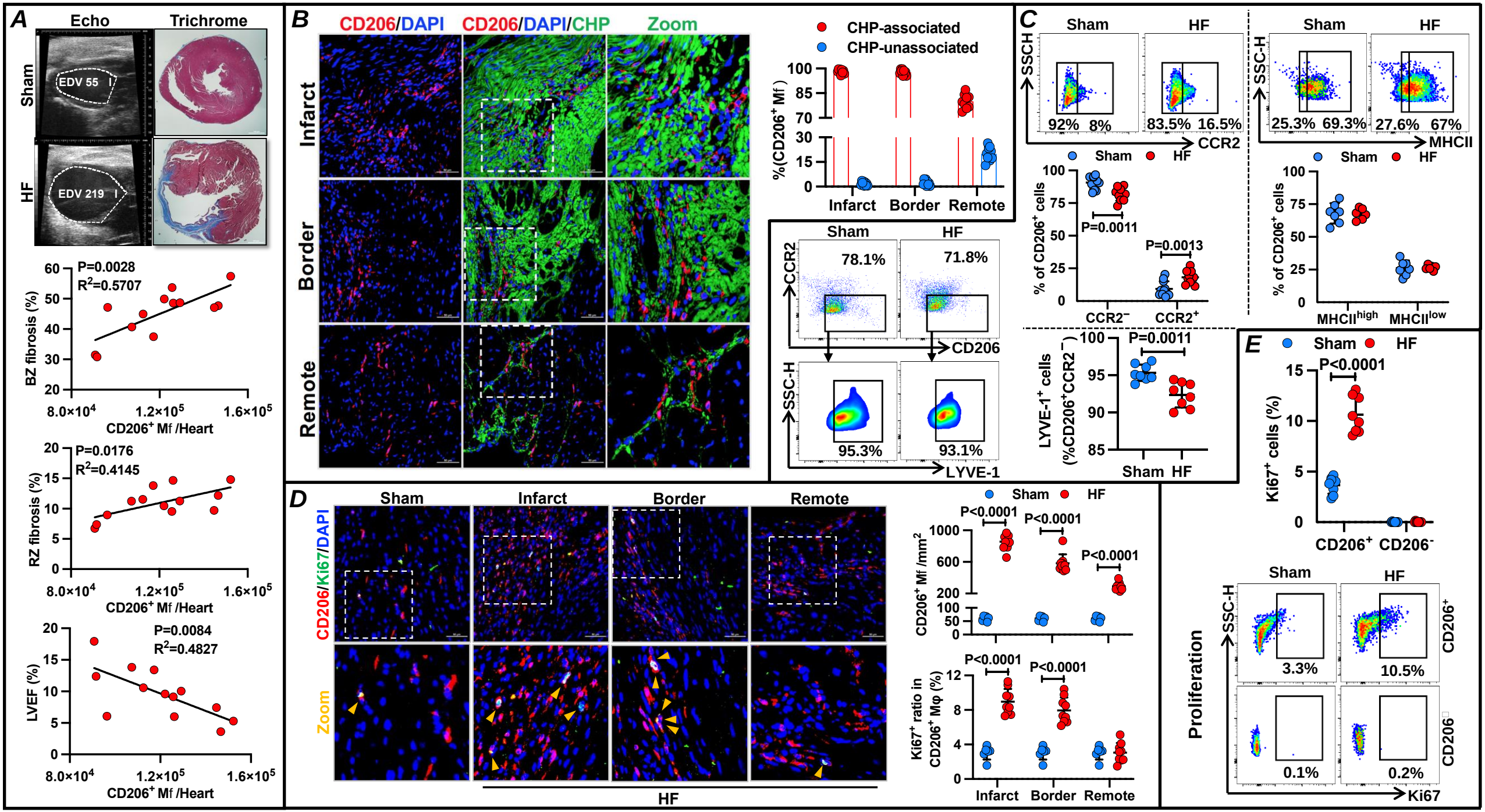
A
Echo
Trichrome
Sham
HF
EDV 55
EDV 219
P=0.0028
R2=0.5707
BZ fibrosis (%)
CD206+ Mf /Heart
P=0.0176
R2=0.4145
RZ fibrosis (%)
P=0.0084
R2=0.4827
LVEF (%)
B
CD206/DAPI
CD206/DAPI/CHP
Zoom
Infarct
Border
Remote
CHP-associated
CHP-unassociated
%(CD206+ Mf)
Infarct Border Remote
CCR2
CD206
78.1%
71.8%
SSC-H
95.3%
93.1%
LYVE-1
C
Sham
HF
SSC
CCR2
92%
8%
83.5%
16.5%
MHCII
25.3%
69.3%
27.6%
67%
% of CD206+ cells
P=0.0011
P=0.0013
CCR2−
CCR2+
MHCIIhigh
MHCIIlow
LYVE-1+ cells (%CD206+CCR2−)
D
CD206/Ki67/DAPI
Zoom
HF
CD206+ Mf /mm2
P<0.0001
Ki67+ ratio in CD206+ Mφ (%)
E
Ki67+ cells (%)
CD206+
CD206-
Proliferation
3.3%
10.5%
0.1%
0.2%
Ki67

Figure 2

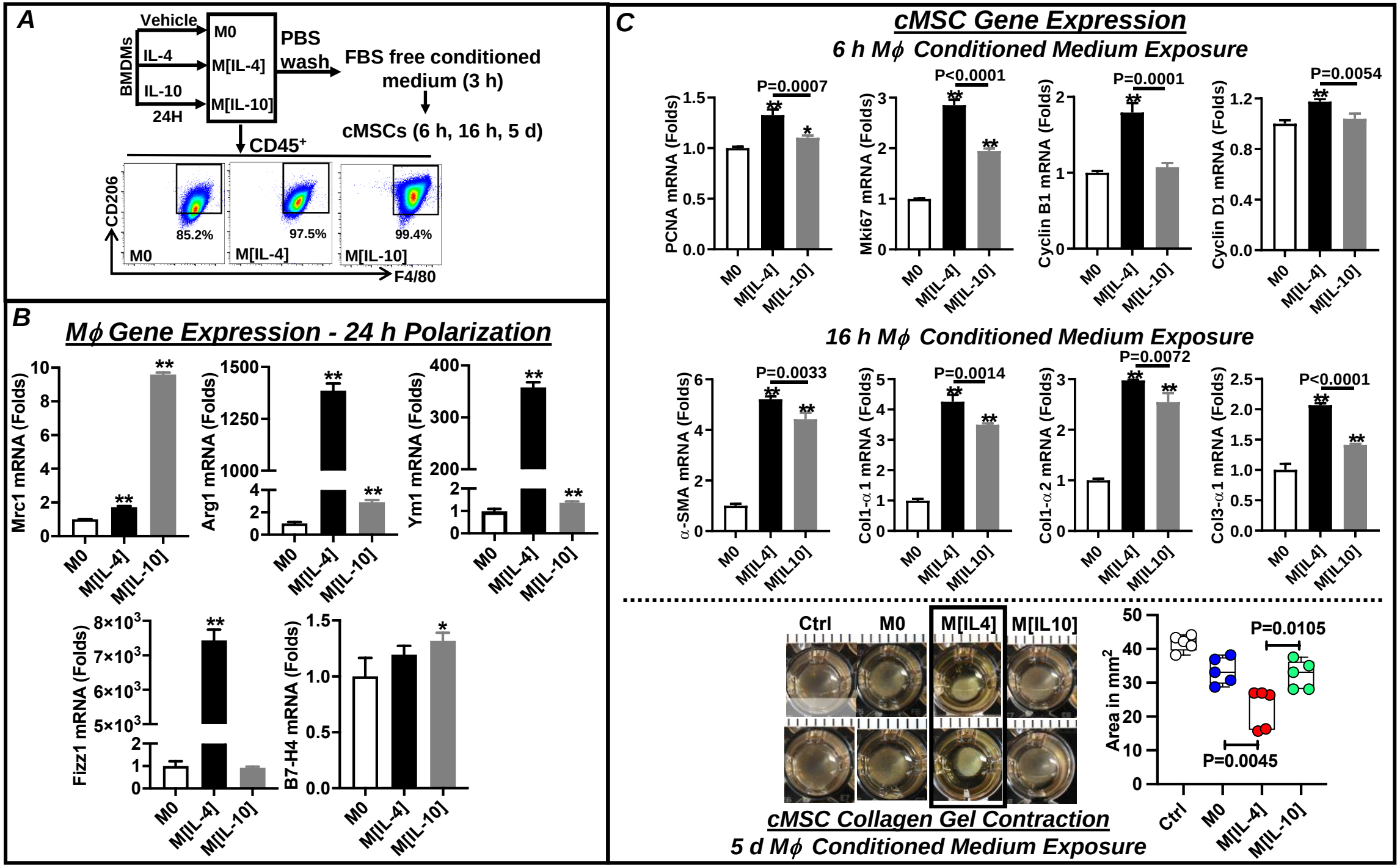
A
Vehicle
IL-4
IL-10
24H
BMDMs
M0
M[IL-4]
M[IL-10]
PBS wash
FBS free conditioned medium (3 h)
cMSCs (6 h, 16 h, 5 d)
CD45+
CD206
F4/80
85.2%
97.5%
99.4%
M0
M[IL-4]
M[IL-10]
B
Mϕ Gene Expression - 24 h Polarization
Mrc1 mRNA (Folds)
Arg1 mRNA (Folds)
Ym1 mRNA (Folds)
Fizz1 mRNA (Folds)
B7-H4 mRNA (Folds)
C
cMSC Gene Expression
6 h Mϕ Conditioned Medium Exposure
PCNA mRNA (Folds)
P=0.0007
Mki67 mRNA (Folds)
P<0.0001
Cyclin B1 mRNA (Folds)
P=0.0001
Cyclin D1 mRNA (Folds)
P=0.0054
16 h Mϕ Conditioned Medium Exposure
α-SMA mRNA (Folds)
P=0.0033
Col1-α1 mRNA (Folds)
P=0.0014
Col1-α2 mRNA (Folds)
P=0.0072
Col3-α1 mRNA (Folds)
P<0.0001
M[IL4]
M[IL10]
Ctrl
M0
M[IL4]
M[IL10]
cMSC Collagen Gel Contraction
5 d Mϕ Conditioned Medium Exposure
Area in mm2
P=0.0105
P=0.0045

Figure 3

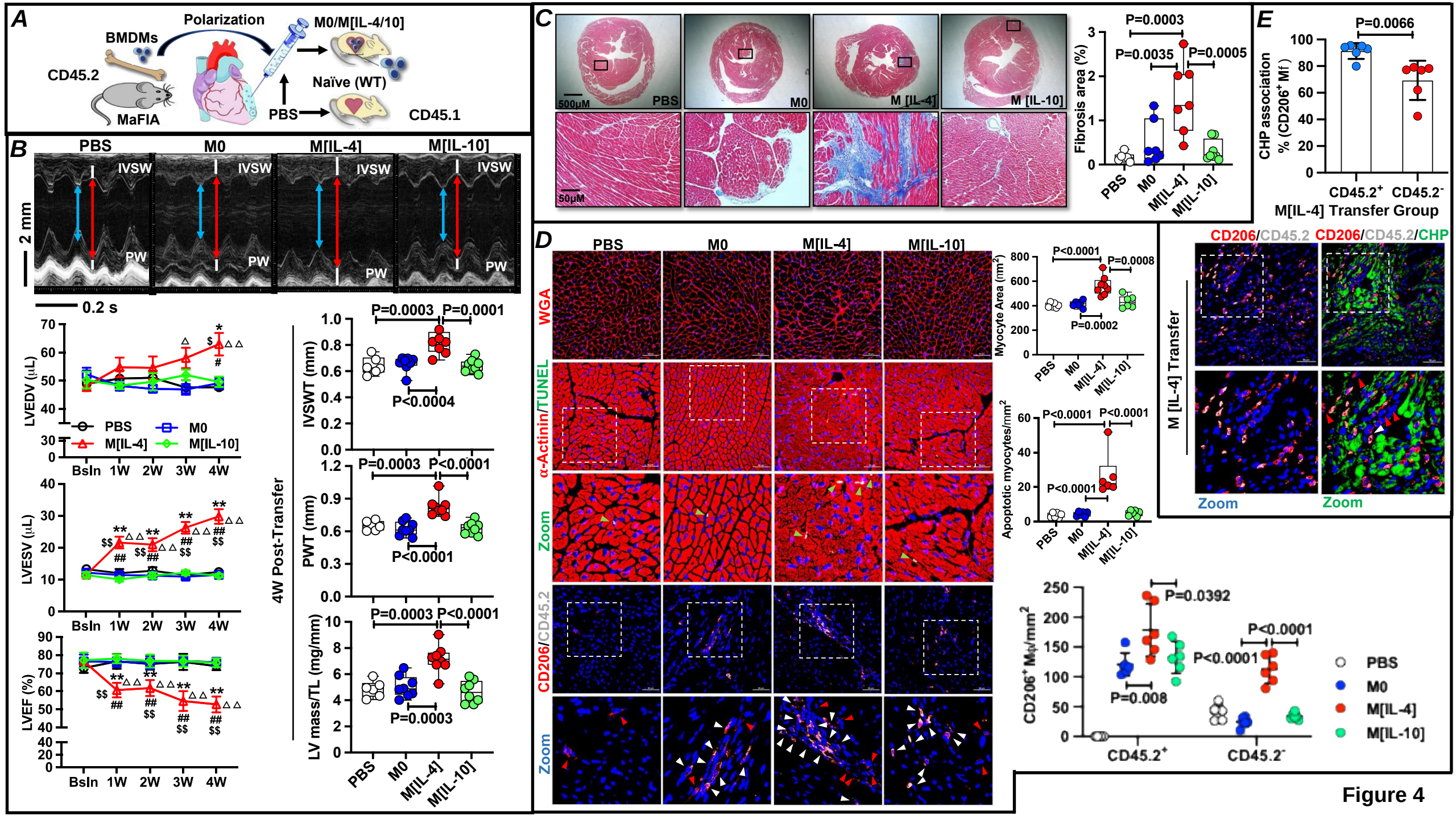
A
Polarization
BMDMs
CD45.2
MaFIA
M0/M[IL-4/10]
Naïve (WT)
PBS
CD45.1
B
PBS
M0
M[IL-4]
M[IL-10]
IVSW
PW
2 mm
0.2 s
LVEDV (μL)
LVESV (μL)
LVEF (%)
BsIn 1W 2W 3W 4W
4W Post-Transfer
IVSWT (mm)
PWT (mm)
LV mass/TL (mg/mm)
P=0.0003 P=0.0001
P<0.0004
P=0.0003 P<0.0001
P<0.0001
P=0.0003 P<0.0001
P=0.0003
C
500μM
50μM
Fibrosis area (%)
P=0.0003
P=0.0035
P=0.0005
D
WGA
α-Actinin/TUNEL
CD206/CD45.2
Zoom
Myocyte Area (mm²)
P<0.0001
P=0.0008
P=0.0002
Apoptotic myocytes/mm²
P<0.0001 P<0.0001
P<0.0001
CD206⁺ Mφ/mm²
P=0.0392
P<0.0001
P<0.0001
P=0.008
CD45.2⁺
CD45.2⁻
E
CHP association % (CD206⁺ Mf)
P=0.0066
CD45.2⁺ CD45.2⁻
M[IL-4] Transfer Group
CD206/CD45.2 CD206/CD45.2/CHP
M [IL-4] Transfer
Zoom

Figure 4

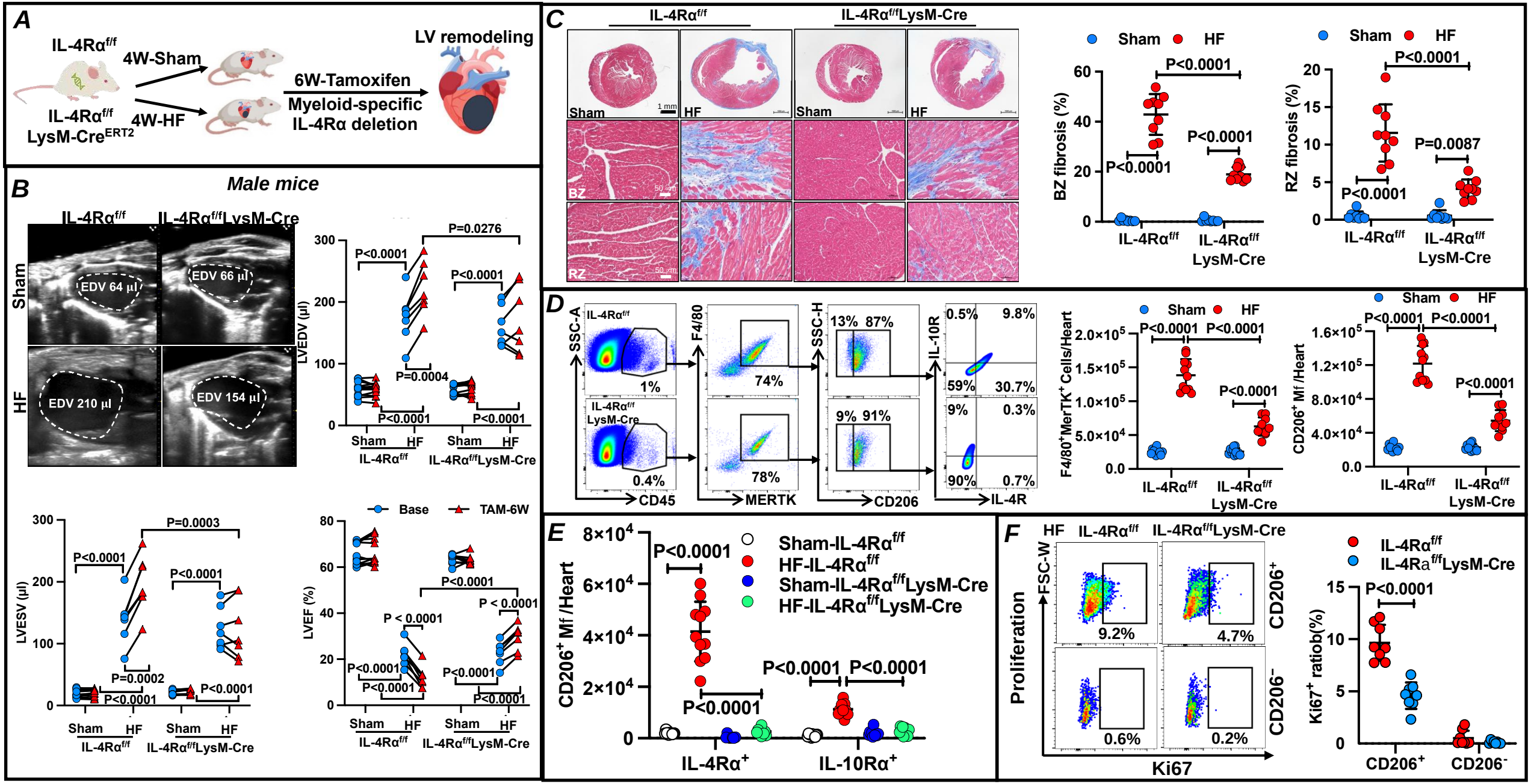
A
IL-4Rα f/f
4W-Sham
IL-4Rα f/f LysM-Cre ERT2
4W-HF
6W-Tamoxifen
Myeloid-specific IL-4Rα deletion
LV remodeling
B
Male mice
IL-4Rα f/f
IL-4Rα f/f LysM-Cre
Sham
HF
EDV 64 µl
EDV 66 µl
EDV 210 µl
EDV 154 µl
LVEDV (µl)
P=0.0276
P<0.0001
P=0.0004
P<0.0001
P<0.0001
P<0.0001
Sham HF
IL-4Rα f/f
IL-4Rα f/f LysM-Cre
LVESV (µl)
P=0.0003
P<0.0001
P<0.0001
P=0.0002
P<0.0001
P<0.0001
Base
TAM-6W
LVEF (%)
P<0.0001
P < 0.0001
P<0.0001
P<0.0001
P < 0.0001
P<0.0001
P<0.0001
C
IL-4Rα f/f
IL-4Rα f/f LysM-Cre
Sham
HF
1 mm
BZ
RZ
50 µm
BZ fibrosis (%)
RZ fibrosis (%)
P<0.0001
P<0.0001
P<0.0001
P<0.0001
P=0.0087
D
IL-4Rα f/f
IL-4Rα f/f LysM-Cre
SSC-A
CD45
1%
0.4%
F4/80
MERTK
74%
78%
SSC-H
CD206
13% 87%
9% 91%
IL-10R
IL-4R
0.5% 9.8%
59% 30.7%
9% 0.3%
90% 0.7%
F4/80+MerTK+ Cells/Heart
CD206+ Mf /Heart
P<0.0001
P<0.0001
P<0.0001
E
CD206+ Mf /Heart
P<0.0001
P<0.0001
Sham-IL-4Rα f/f
HF-IL-4Rα f/f
Sham-IL-4Rα f/f LysM-Cre
HF-IL-4Rα f/f LysM-Cre
P<0.0001 P<0.0001
IL-4Rα+
IL-10Rα+
F
HF
IL-4Rα f/f
IL-4Rα f/f LysM-Cre
Proliferation
FSC-W
Ki67
9.2%
4.7%
0.6%
0.2%
CD206+
CD206-
IL-4Rα f/f
IL-4Rα f/f LysM-Cre
Ki67+ ratiob(%)
P<0.0001
CD206+
CD206-

Figure 5

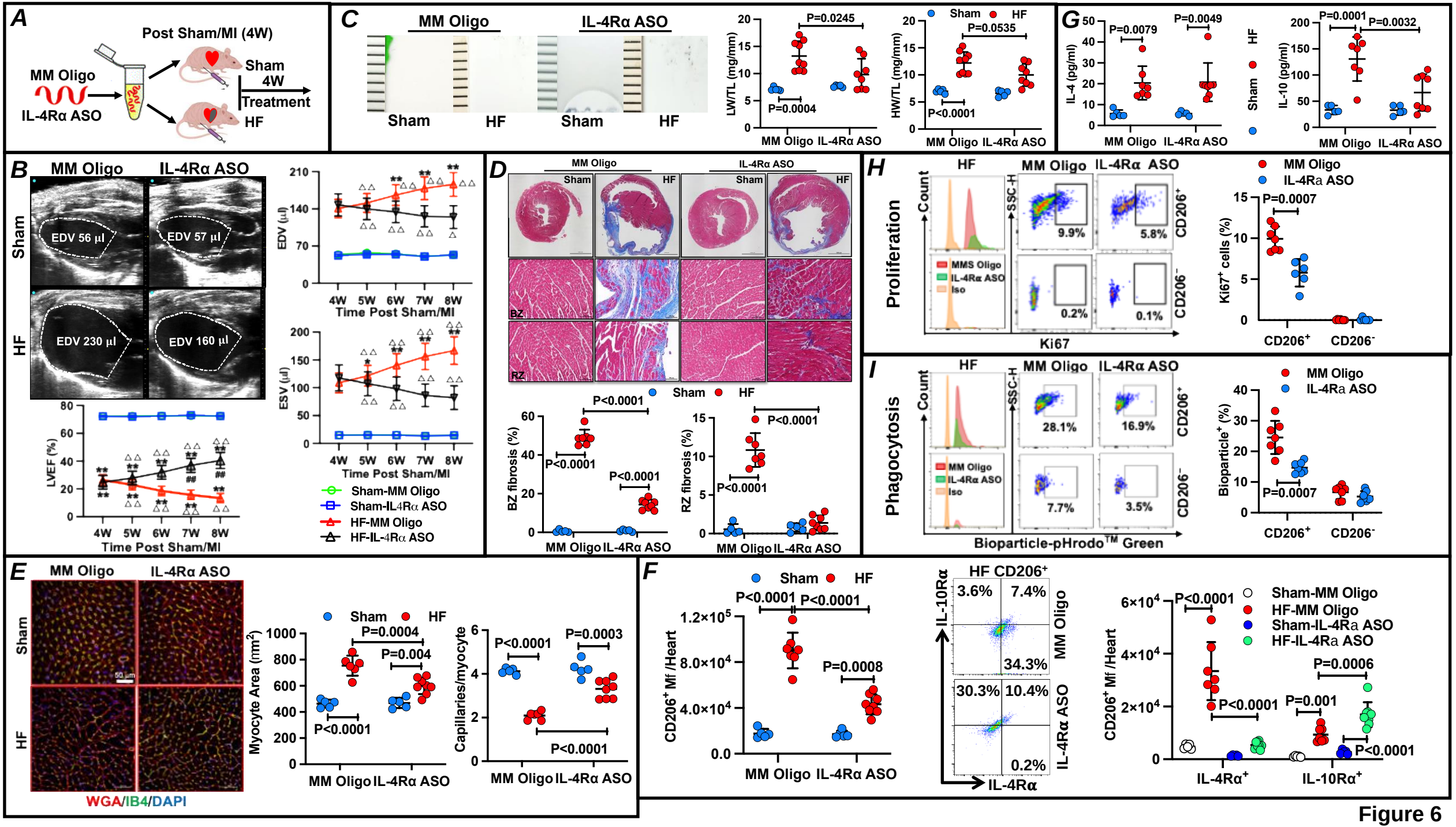
A
Post Sham/MI (4W)
MM Oligo
IL-4Rα ASO
Sham
4W
Treatment
HF
B
MM Oligo
IL-4Rα ASO
Sham
HF
EDV 56 μl
EDV 57 μl
EDV 230 μl
EDV 160 μl
LVEF (%)
Time Post Sham/MI
EDV (μl)
ESV (μl)
Sham-MM Oligo
Sham-IL4Rα ASO
HF-MM Oligo
HF-IL-4Rα ASO
C
MM Oligo
IL-4Rα ASO
Sham
HF
LW/TL (mg/mm)
HW/TL (mg/mm)
P=0.0245
P=0.0004
P=0.0535
P<0.0001
D
BZ
RZ
BZ fibrosis (%)
RZ fibrosis (%)
P<0.0001
P<0.0001
E
WGA/IB4/DAPI
Myocyte Area (㎛²)
Capillaries/myocyte
P=0.0004
P=0.004
P<0.0001
P=0.0003
F
CD206⁺ Mf /Heart
P=0.0008
HF CD206⁺
IL-10Rα
IL-4Rα
3.6%
7.4%
34.3%
30.3%
10.4%
0.2%
Sham-MM Oligo
HF-MM Oligo
Sham-IL-4Ra ASO
HF-IL-4Ra ASO
P=0.0006
P=0.001
IL-4Rα⁺
IL-10Rα⁺
G
IL-4 (pg/ml)
IL-10 (pg/ml)
P=0.0079
P=0.0049
P=0.0001
P=0.0032
H
Proliferation
MMS Oligo
IL-4Rα ASO
Iso
Ki67
9.9%
5.8%
0.2%
0.1%
Ki67⁺ cells (%)
P=0.0007
I
Phagocytosis
MM Oligo
IL-4Rα ASO
Iso
Bioparticle-pHrodo™ Green
28.1%
16.9%
7.7%
3.5%
Bioparticle⁺ (%)
P=0.0007

Figure 6

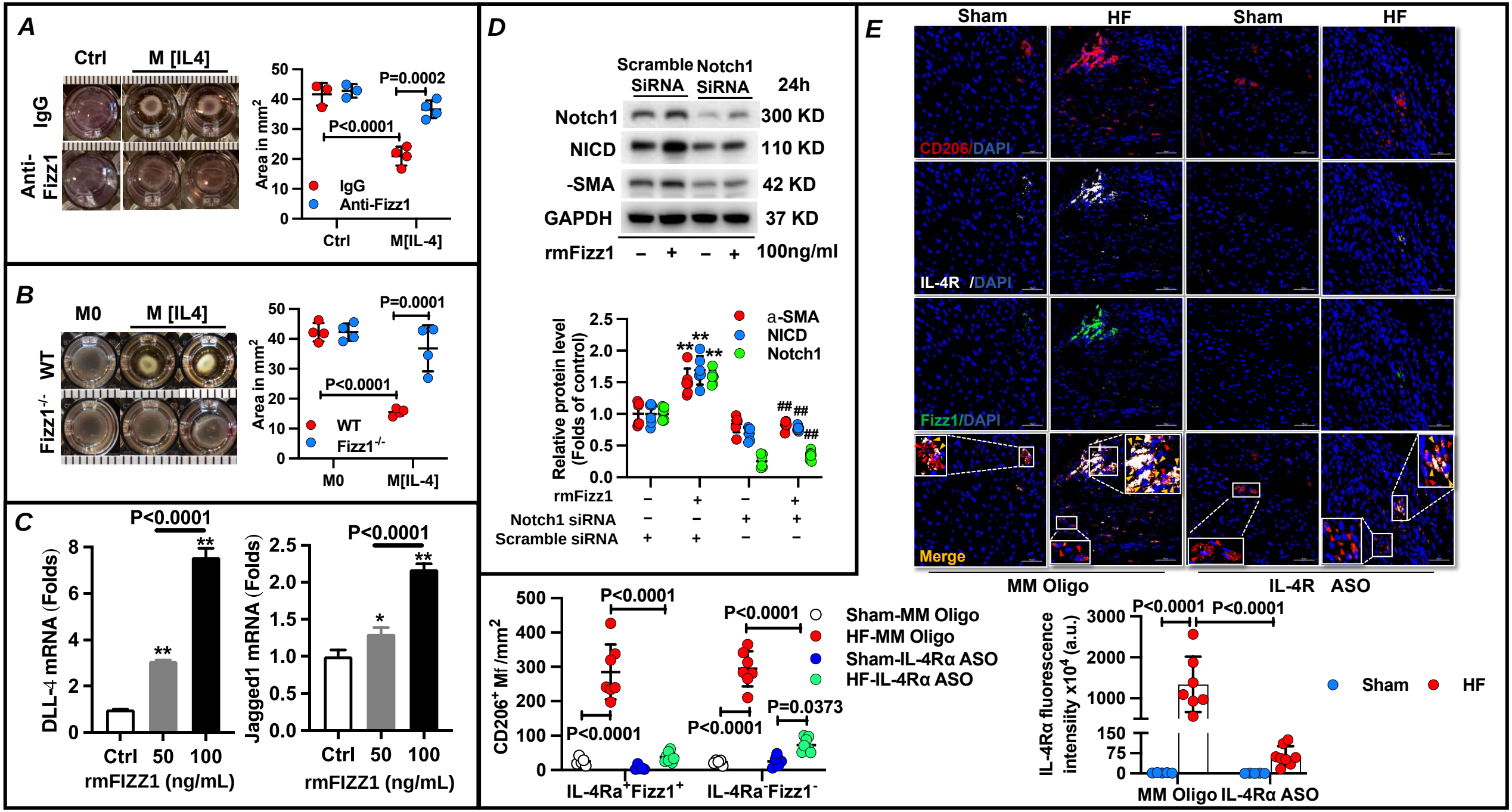
A
Ctrl
M [IL4]
IgG
Anti-Fizz1
Area in mm2
P=0.0002
P<0.0001
IgG
Anti-Fizz1
Ctrl
M[IL-4]
B
M0
M [IL4]
WT
Fizz1-/-
P=0.0001
P<0.0001
WT
Fizz1-/-
M0
M[IL-4]
C
DLL-4 mRNA (Folds)
P<0.0001
Ctrl 50 100
rmFIZZ1 (ng/mL)
Jagged1 mRNA (Folds)
P<0.0001
Ctrl 50 100
rmFIZZ1 (ng/mL)
D
Scramble SiRNA
Notch1 SiRNA
24h
Notch1
NICD
-SMA
GAPDH
300 KD
110 KD
42 KD
37 KD
rmFizz1
100ng/ml
Relative protein level (Folds of control)
a-SMA
NICD
Notch1
rmFizz1
Notch1 siRNA
Scramble siRNA
E
Sham
HF
Sham
HF
CD206/DAPI
IL-4R /DAPI
Fizz1/DAPI
Merge
MM Oligo
IL-4R ASO
CD206+ Mf /mm2
P<0.0001
P<0.0001
P<0.0001
P<0.0001
P=0.0373
IL-4Ra+Fizz1+
IL-4Ra-Fizz1-
Sham-MM Oligo
HF-MM Oligo
Sham-IL-4Rα ASO
HF-IL-4Rα ASO
IL-4Rα fluorescence intensity x10^4 (a.u.)
P<0.0001
P<0.0001
MM Oligo
IL-4Rα ASO
Sham
HF

Figure 7

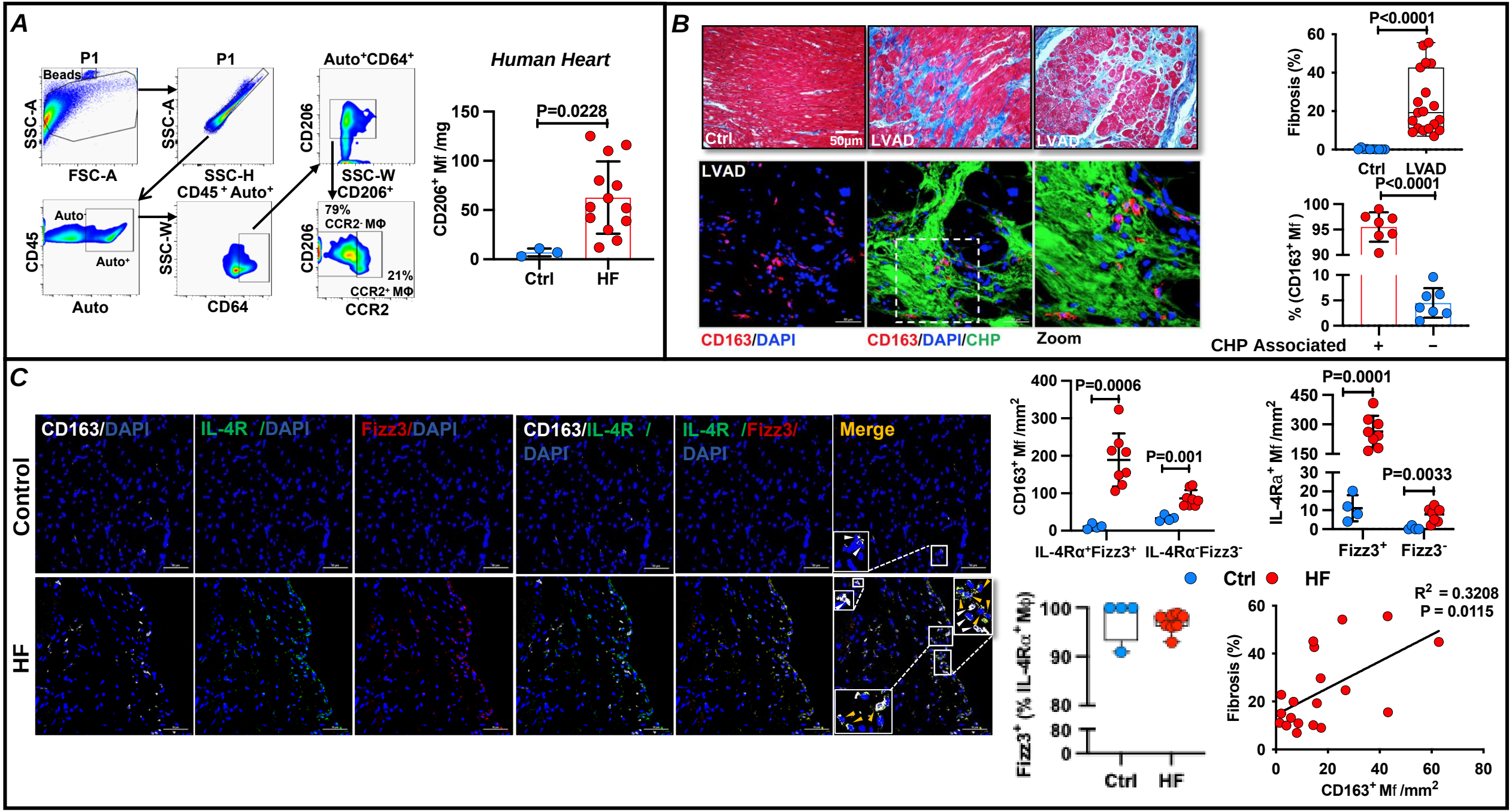
A
P1
Beads
SSC-A
FSC-A
P1
SSC-A
SSC-H
CD45+ Auto+
Auto+CD64+
CD206
SSC-W
CD206+
79%
CCR2- MΦ
21%
CCR2+ MΦ
CD206
CCR2
CD45
Auto
Auto+
Auto
SSC-W
CD64
Human Heart
P=0.0228
CD206+ Mf /mg
150
100
50
0
Ctrl
HF
B
Ctrl
50μm
LVAD
LVAD
LVAD
CD163/DAPI
CD163/DAPI/CHP
Zoom
P<0.0001
Fibrosis (%)
60
40
20
0
Ctrl
LVAD
P<0.0001
% (CD163+ Mf)
100
95
90
10
5
0
CHP Associated
+
–
C
Control
HF
CD163/DAPI
IL-4R /DAPI
Fizz3/DAPI
CD163/IL-4R / DAPI
IL-4R /Fizz3/ DAPI
Merge
P=0.0006
P=0.001
CD163+ Mf /mm2
400
300
200
100
0
IL-4Rα+Fizz3+
IL-4Rα-Fizz3-
P=0.0001
P=0.0033
IL-4Rα+ Mf /mm2
450
300
150
30
20
10
0
Fizz3+
Fizz3-
Fizz3+ (% IL-4Rα+ Mϕ)
100
90
80
80
0
Ctrl
HF
Ctrl
HF
R2 = 0.3208
P = 0.0115
Fibrosis (%)
60
40
20
0
0
20
40
60
80
CD163+ Mf /mm2

Figure 8